JAERI-M
84-071

X-RAY PHOTOELECTRON AND X-RAY-INDUCED AUGER ELECTRON SPECTROSCOPIC DATA, II

—4d TRANSITION-METALS (Y, Zr, Nb, Mo, Ru) AND RELATED OXIDES —

April 1984

Yuji BABA and Teikichi A. SASAKI

日本原子力研究所
Japan Atomic Energy Research Institute

JAERI-Mレポートは，日本原子力研究所が不定期に公刊している研究報告書です。
入手の問合わせは，日本原子力研究所技術情報部情報資料課（〒319-11茨城県那珂郡東海村）あて，お申しこしください。なお，このほかに財団法人原子力弘済会資料センター（〒319-11 茨城県那珂郡東海村日本原子力研究所内）で複写による実費頒布をおこなっております。

JAERI-M reports are issued irregularly.
Inquiries about availability of the reports should be addressed to Information Section, Division of Technical Information, Japan Atomic Energy Research Institute, Tokai-mura, Naka-gun, Ibaraki-ken 319-11, Japan.

編集兼発行　日本原子力研究所
印　　刷　㈱高野高速印刷

JAERI-M 84-071

X-RAY PHOTOELECTRON AND X-RAY-INDUCED AUGER ELECTRON SPECTROSCOPIC DATA, II — 4d TRANSITION-METALS (Y, Zr, Nb, Mo, Ru) AND RELATED OXIDES —

Yuji BABA and Teikichi A. SASAKI

Department of Chemistry, Tokai Research Establishment, JAERI

(Received March 8, 1984)

The intrinsic data of the X-ray photoelectron spectra (XPS) and X-ray-induced Auger electron spectra (XAES) for 4d transition-metals and related oxides were obtained by means of a spherical electron spectrometer. The metallic surfaces were cleaned by two different methods : mechanical filing and Ar^+ ion etching. In the case of the Ar^+ ion bombarded Y, Zr, and Nb metals, the binding energies of the core-lines and the kinetic energies of the Auger lines shift from those for the mechanically filed surfaces. The energy shifts were interpreted in terms of the ion-induced lattice distortion of the metal surfaces. The oxides examined are typical compounds such as Y_2O_3, ZrO_2, Nb_2O_5, MoO_3 and RuO_2. The data consists of 4 wide scans, 33 core-line spectra, 10 valence-band spectra and 12 XAES spectra. The peak positions of the core-lines and the Auger lines were summarized in 6 tables together with their chemical shifts.

KEYWORDS:

X-ray Photoelectron Spectroscopy, X-ray-induced Auger Electron Spectroscopy, Yttrium, Zirconium, Niobium, Molybdenum, Ruthenium, Y_2O_3, ZrO_2, Nb_2O_5, MoO_3, RuO_2, Sputtering

---

This work was done by the use of an ESCA spectrometer connected with the JAERI Tandem Accelerator.

X線光電子及びX線励起オージェ電子スペクトルデータ Ⅱ
－4d遷移金属（Y，Zr，Nb，Mo，Ru）及びその酸化物－

日本原子力研究所東海研究所原子炉化学部
馬場 祐治・佐々木 貞吉

（１９８４年３月８日受理）

４ｄ遷移金属とその酸化物について，半球型電子エネルギー分析器によりＸ線光電子分光スペクトル（ＸＰＳ）及びX線励起オージェ電子スペクトル（ＸＡＥＳ）を測定した。金属の真正表面は，２通りの異なる方法，すなわち超高真空中やすり研摩法及びアルゴンイオンエッチング法で得た。アルゴンイオン照射した金属試料では，内殻電子の結合エネルギー及びオージェ電子の運動エネルギーは，やすり研摩した場合と異なった値を示す。このエネルギーシフトは，イオン照射で誘起された結晶格子の表面損傷によると考えられる。また，Y_2O_3，ZrO_2，Nb_2O_5，MoO_3，RuO_2などの酸化物についても測定を行った。本報は４種のワイドスキャン，３３種の内殻スペクトル，１０種の価電子帯スペクトル及び１２種のＸＡＥＳスペクトルから成る。内殻電子の結合エネルギー，オージェ電子の運動エネルギー及びオージェパラメーターは，化学シフトと共に表にまとめた。

CONTENTS

目　　次

LIST OF TABLES

---

* Notation *fl* indicates a mechanical filing.

** Notation *et* indicates an Ar^+ ion etching.

LIST OF FIGURES

1. Introduction

This report presents the intrinsic data of the X-ray photoelectron spectroscopy (XPS) and X-ray-induced Auger electron spectroscopy (XAES) for some 4d transition-metals and their typical oxides. The objects of this report are essentially the same as those described in our previous work dealing with 3d transision-metals.[1)]

Briefly, the first is to present the XPS spectra which have not been compiled in handbook,[2)] such as valence-band spectra and core-line spectra with relatively weak intensities. The second is to display the intrinsic XAES spectra, since there has been no available data for the XAES analysis. The third, which is especially emphasized in this report, is to elucidate the spectral difference between metal surfaces etched with Ar^+ ions and those obtained by mechanical filing. The observed differences were interpreted in terms of the lattice distortion of the metal surfaces.

2. Preparation of samples

Starting materials used were 99.9 % metallic foils. The clean surfaces of the metals were obtained by two different methods. One is a mechanical filing in a preparation chamber under the pressure of 1.3×10^{-8} Pa, and another is an Ar^+ ion etching. The latter was done by bombarding the mechanically filed metals with 8 keV Ar^+ ions at a current density of 10 $\mu A/cm^2$. Figure 1 shows the energy shifts of the $Nb3d_{5/2}$ line for the Ar^+ ion bombarded Nb metal as a function of the ion fluence. The separation energy is almost proportional to the ion fluence upto $\sim 2\times10^{16}$ ions/cm^2, whereas it saturates at the fluence over $\sim 6\times10^{16}$ ions/cm^2. On the basis of this observation, the Ar^+ ion bombardment for the compiled data was carried out at the total fluence upto $\sim 10^{17}$ ions/cm^2.

The oxides such as Y_2O_3, ZrO_2, Nb_2O_5, and MoO_3 were prepared by oxidizing the metallic foils at 300-400°C in an oxygen atmosphere, and RuO_2 was obtained by ignizing metallic powder at 900°C in oxygen atmosphere. Before the spectral measurements, the samples were heated upto 200°C in the spectrometer chamber under the pressure of $\sim 1.3\times10^{-7}$ Pa.

3. Spectral measurements

The XPS and XAES measurements were carried out by means of a V.G. ESCALAB-5 spectrometer equipped with a spherical electron analyzer. The base pressure during the measurements was less than 1.3×10^{-8} Pa. A Mg Kα X-ray source (1253.6 eV) was operated at 125 W. The spectrometer was calibrated such that the $Au4f_{7/2}$ line appears at E_b=84.0 eV. The FWHM (full-width at half maximum) of the $Au4f_{7/2}$ line was 0.9 eV, and the reproducibility of the spectrometer was within ±0.1 eV. In the case of the insulating oxides, the original spectra shifted to the higher binding-energy side because of the charging effect. Therefore, the energy scale was aligned to make the peak positions of the metal $3d_{3/2}$ lines for the oxides and for the most oxidized species on the oxygen-adsorbed metallic surfaces coinside.

4. Data interpretation

4. 1 General description

In the tables and figures, the notations *fl* and *et* indicate the procedures of the mechanical filing and Ar^+ ion etching, respectively. The XPS and XAES spectra for Y_{fl}, Y_{et} and Y_2O_3 are presented in Figs. 2-15, for Zr_{fl}, Zr_{et} and ZrO_2 in Figs. 16-27, for Nb_{fl}, Nb_{et} and Nb_2O_5 in Figs. 28-41, for Mo_{fl}, Mo_{et} and MoO_3 in Figs. 42-57, and for RuO_2 in Figs. 58-60, respectively. In these figures, the peak position is indicated in eV. The binding energies of the core-lines are summarized in Tables 1-5 and the kinetic energies of the Auger lines are listed in Table 6.

4. 2 Metal surfaces

The binding energies of the core-lines for Y_{et}, Zr_{et}, and Nb_{et} shifted to the higher binding energy side by 0.1-1.0 eV from those for the corresponding metallic surfaces obtained by mechanical filing. These core-line shifts have been observed in such metals as Pd,[3] Ti,[1] and V.[1]

The kinetic energis of the Auger-lines for Y_{et}, Zr_{et} and Nb_{et} also shifted to the lower kinetic energy side by 0.9-1.7 eV. It is apparent that these energy shifts are not due to the surface oxides, since the spectral intensity of the O1s area remained unchanged after the Ar^+ ion bombardment.

One of the plausible reasons of the energy shifts may be the radiation damage induced by the Ar^+ ion bombardment. In fact, it has been observed that the bombardment with heavy-ions causes the surface roughness such as cone formation.[4-6] Although the quantitative explanation of the ion-induced damages has not been given, an importance of the nucleation and growth of the vacancy clusters in the surface layer was pointed out.[7,8] In this model, the ion-induced vacancies in the surface layer agglomerate by diffusion resulting in the formation of the porous metal surfaces.

On the other hand, the core-line energies seem to be related to the atomic density of the sample. In practice, the binding energies of the gas phase for the transition-metals shift to the higher energy side by 2-4 eV from those of the solid phase.[9,10] Thus, the core-line shift to the higher energy side for the ion bombarded metal is presumably associated with the formation of the porous surfaces whose atomic density is relatively small compared with the original metals. To confirm this assumption, we have measured the XPS spectra for porous Nb metal obtained by the following procedure.

First, the niobium hydride $NbH_{0.86}$ was thermally synthesized in the electric furnace by the direct reaction of Nb metal with hydrogen at 570°C. The hydride was then dehydrogenated at 1100°C under the high vacuum. By this treatment, the $Nb3d_{5/2}$ line was moved to 202.6 eV, which is higher by 0.2 eV than that for Nb_{fl}. Since there exists no phase transition of Nb metal below the melting point, i.e., 2400°C,[11] the dehydrogenated Nb metal may preserve the crystal structure of hydride. The phenomenon is similar to the result of the Ar^+ ion bombarded surfaces, though the energy shift is smaller compared with that for Nb_{et}. Such an energy discrepancy between dehydrogenated and filed metals was also observed for vanadium system. The $V2p_{3/2}$ line for dehydrogenated vanadium appears at 512.4 eV, which is higher by 0.3 eV from that for V_{fl}.

Considering the results mentioned above, it should be careful to use the data for the sputtered surface as an energy reference of chemical

shifts in such metals as Ti,[1] V,[1] Y, Zr, and Nb. On the other hand, the energy shifts were not observed in Sc,[1] Ni,[1] and Mo, upto the total fluence of $\sim 10^{18}$ ions/cm^2. In the present stage, we cannot give conclusive explanation to the present results that the energy shift of the Ar^+ ion bombarded Nb metal is the largest in all the metals examined. However, it is evident that the metals which give appreciable energy shifts are those easily absorbing hydrogen to form relatively stable hydride and having the porous metal structure after dehydrogenation.

4. 3 Oxides

The binding energies or the chemical shifts of the main core-lines are almost same as those previously reported for Y_2O_3,[12] ZrO_2,[12] Nb_2O_5,[12-15] and MoO_3.[12,16-18]

Although the chemical shifts of the Auger lines had long been considered to be almost same as those of the corresponding core-lines, it has been found that these two energy shifts are often different because of difference in the extra-atomic relaxation energy.[10] The separation between the Auger line and the core-line reflects the extra-atomic relaxation energy. This has been called the Auger parameter α,[10] and defined as a following equation,

$$\alpha = KE_A - KE_p$$

$$= KE_A + BE_p - h\upsilon$$

where KE and BE represent the kinetic energy and the binding energy, the suffix A and p represent the Auger electron and photoelectron, respectively, and $h\upsilon$ is the exciting X-ray energy. Using the Auger parameter, the charging effect which is often observed in the spectroscopic measurements of the insulating samples can be canceled. Another experimental advantage of the use is that the correction of the work function is not necessary, and the measured values can be directly compared with those obtained by the other investigators.

The Auger parameters for the oxides and their shifts from those of the

metallic states obtained by the mechanical filing are given in Table 7. In Nb and Mo system, the large chemical shifts of both the $3d_{5/2}$ lines and $M_{4,5}N_{2,3}V$ Auger lines are canceled. Since $\Delta\alpha$ from the metallic state decreases with the polarization of the chemical bond,[10] the values for Nb_2O_5 and MoO_3 indicate the large polarization of the metal-O bonds in these oxides.

REFERENCES

1) Baba Y. and Sasaki T. A. : JAERI-M 84-005, Japan Atomic Energy Research Institute (1984).
2) Wagner C. D., Riggs W. M., Davis L. E., Moulder J. F. and Mullenberg G. E. : "Handbook of X-ray Photoelectron Spectroscopy", Perkin-Elmer Corporation, Minnesota (1979).
3) Hüfner S., Wertheim G. K. and Buchanan D. N. E. : Chem. Phys. Lett., 24, 527 (1974).
4) Wehner G. K. and Hajicek D. J. : J. Appl. Phys., 42, 1145 (1971).
5) Tsunoyama K., Suzuki T. and Ohashi Y. : Japanese J. Appl. Phys., 15, 349 (1976).
6) Bhatia C. S. : Thin Solid Films, 96, 249 (1982).
7) Cherns D. : Phil. Mag., 36, 1429 (1977).
8) Verheij L. K., Van den Berg J. A. and Armour D. G. : Surf. Sci., 122, 216 (1982).
9) Ley L., Kowalczyk S. P., McFeely F. R., Pollak R. A. and Shirley D. A. : Phys. Rev. B, 8, 3583 (1973).
10) Wagner C. D. : Faraday Discuss. Chem. Soc., 60, 291 (1975).
11) For example see Miller G. L. : "Tantalum and Niobium", Butterworths Scientific Publication, London (1959), p372.
12) Nefedov V. I., Gati D., Dzhurinskii B. F., Sergushin N. P. and Salyn Ya. V. : Zh. Neorg. Khim., 20, 2307 (1975).
13) McGuire G. E., Schweitzer G. K. and Carlson T. A. : Inorg. Chem., 12, 2451 (1973).
14) Simon D., Perrin C. and Baillif P. : C. R. Acad. Sci. Paris, C 241, 283 (1976).
15) Fontaine R., Cailiat R., Feve L. and Guittet M. J. : J. Electron Spectrosc., 10, 349 (1977).
16) Grim S. O. and Matienzo L. J. : Inorg. Chem., 14, 1015 (1975).
17) Patterson T. A., Carver J. C., Leyden D. E. and Hercules D. M. : J. Phys. Chem., 80, 1702 (1976).
18) Ivanov I. K., Kostikov Yu. P., Korol'kov D. V. and Avramekov A. G. : Zh. Obshch. Khim., 47, 1189 (1977).

Table 1 Binding energies and chemical shifts of the core-lines for Y_{fl}, Y_{et} and Y_2O_3.

Sample	Orbital	E_b (eV)	Chemical Shift (eV)	Fig. No.
Y_{fl}	3s	395.4	-	3
	$3p_{3/2}$	299.3	-	4
	$3d_{3/2}$	157.9	-	5
	$3d_{5/2}$	155.9	-	5
	4p	24.1	-	6
Y_{et}	$3d_{3/2}$	158.2	0.3	9
	$3d_{5/2}$	156.1	0.2	9
Y_2O_3	3s	396.1	0.7	11
	$3p_{3/2}$	301.6	2.3	12
	$3d_{3/2}$	160.5	2.6	13
	$3d_{5/2}$	158.6	2.7	13

Table 2 Binding energies and chemical shifts of the core-lines for Zr_{fl}, Zr_{et} and ZrO_2.

Sample	Orbital	E_b (eV)	Chemical Shift (eV)	Fig. No.
Zr_{fl}	3s	430.2	-	17
	$3p_{3/2}$	329.9	-	18
	$3d_{3/2}$	181.4	-	19
	$3d_{5/2}$	179.0	-	19
	4p	27.5	-	20
Zr_{et}	$3d_{3/2}$	181.5	0.1	23
	$3d_{5/2}$	179.2	0.2	23
ZrO_2	$3d_{3/2}$	185.5	4.1	25
	$3d_{5/2}$	183.3	4.3	25

Table 3 Binding energies and chemical shifts of the core-lines for Nb_{fl}, Nb_{et} and Nb_2O_5.

Sample	Orbital	E_b (eV)	Chemical Shift (eV)	Fig. No.
Nb_{fl}	3s	467.1	-	29
	$3p_{3/2}$	360.7	-	30
	$3d_{3/2}$	205.2	-	31
	$3d_{5/2}$	202.4	-	31
	4p	31.0	-	32
Nb_{et}	$3p_{3/2}$	361.7	1.0	35
	$3d_{3/2}$	205.7	0.5	36
	$3d_{5/2}$	203.0	0.6	36
Nb_2O_5	$3d_{3/2}$	210.7	5.5	39
	$3d_{5/2}$	208.1	5.7	39

Table 4 Binding energies and chemical shifts of the core-lines for Mo_{fl}, Mo_{et} and MoO_3.

Sample	Orbital	E_b (eV)	Chemical Shift (eV)	Fig. No.
Mo_{fl}	3s	506.3	-	43
	$3p_{3/2}$	394.0	-	44
	$3d_{3/2}$	231.1	-	45
	$3d_{5/2}$	228.0	-	45
	4s	62.6	-	46
	4p	35.6	-	47
Mo_{et}	$3d_{3/2}$	231.1	0.0	50
	$3d_{5/2}$	227.9	-0.1	50
MoO_3	3s	511.0	4.7	52
	$3p_{3/2}$	398.6	4.6	53
	$3d_{3/2}$	235.8	4.7	54
	$3d_{5/2}$	232.7	4.7	54
	4p	40.4	4.8	55

Table 5 Binding energies of the core-lines for RuO_2.

Orbital	E_b (eV)	Fig. No.
$3p_{3/2}$	463.0	58
$3d_{3/2}$	285.4	59
$3d_{5/2}$	281.2	59

Table 6 Kinetic energies and chemical shifts of the $M_{4,5}N_{2,3}V$ Auger lines for Y, Zr, Nb, Mo and their compounds.

Sample	E_k (eV)	Chemical Shift (eV)	Fig. No.
Y_{fl}	124.3	-	8
Y_{et}	123.4	0.9	10
Y_2O_3	117.8	6.5	15
Zr_{fl}	148.6	-	22
Zr_{et}	147.3	1.3	24
ZrO_2	141.9	6.7	27
Nb_{fl}	167.8	-	34
Nb_{et}	166.1	1.7	38
Nb_2O_5	161.6	6.2	41
Mo_{fl}	187.0	-	49
Mo_{et}	187.1	-0.1	51
MoO_3	182.0	5.0	57

Table 7 Auger parameters and their shifts from metallic states for Y, Zr, Nb, Mo and their oxides.

Sample	α (eV)	Δα (eV)
Y	-973.4	-
Y_2O_3	-977.2	3.8
Zr	-926.0	-
ZrO_2	-928.4	2.4
Nb	-883.4	-
Nb_2O_5	-883.9	0.5
Mo	-838.6	-
MoO_3	-838.9	0.3

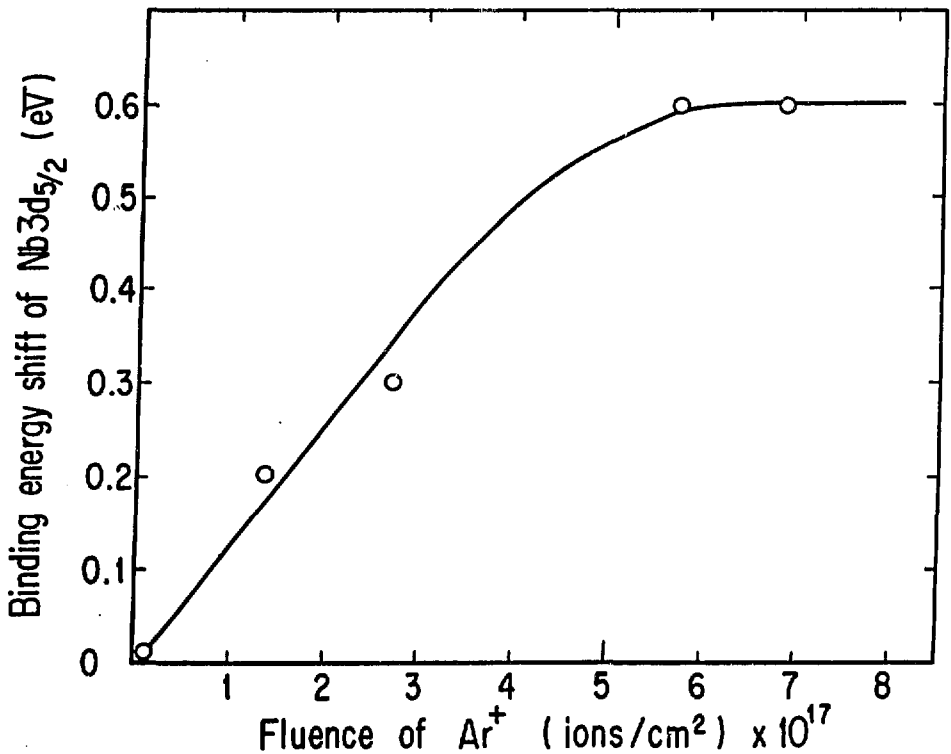

Fig. 1 Binding energy shifts of $Nb3d_{5/2}$ line for Ar^+ ion bombarded Nb metal as a function of ion fluence.

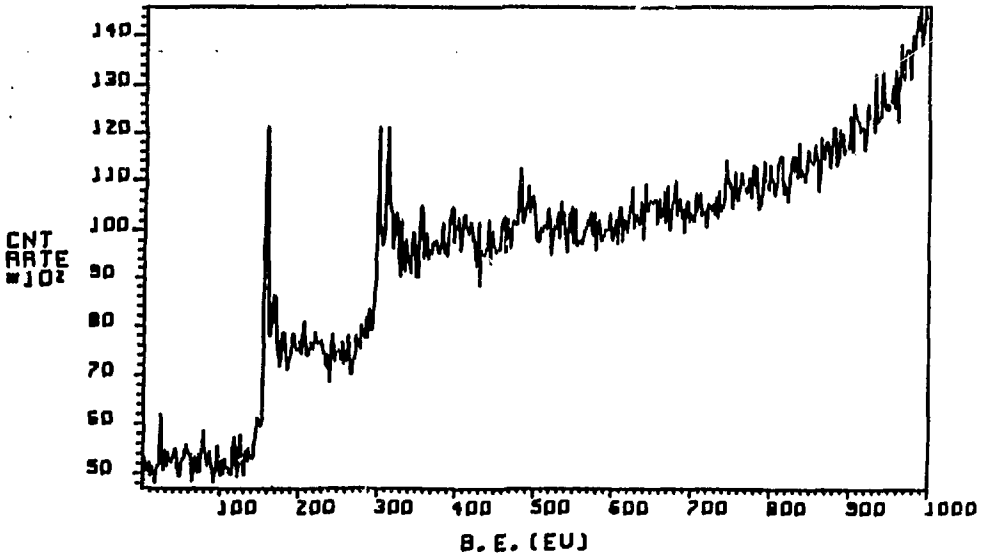

Fig. 2 XPS wide scan of Y_{fl}.

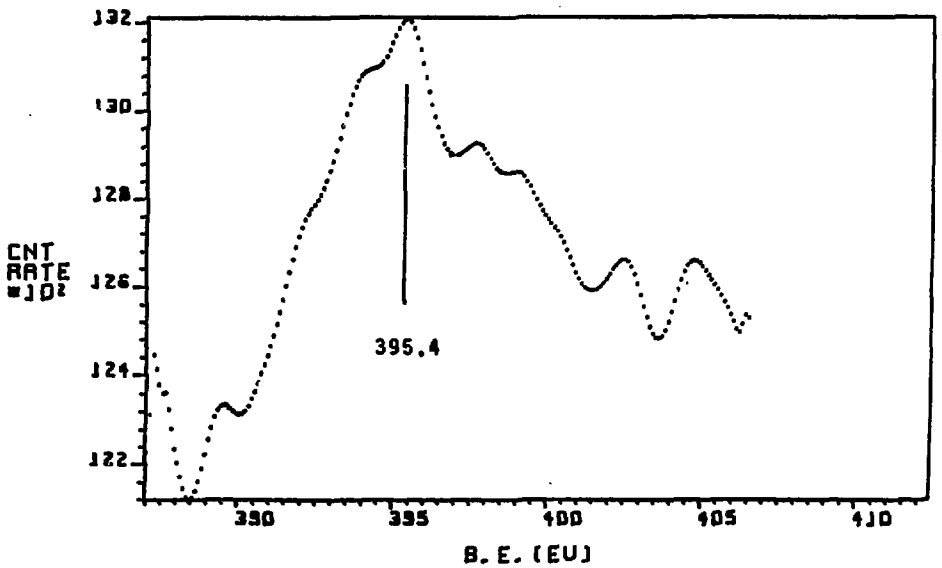

Fig. 3 Y3s XPS spectrum of Y_{fl}.

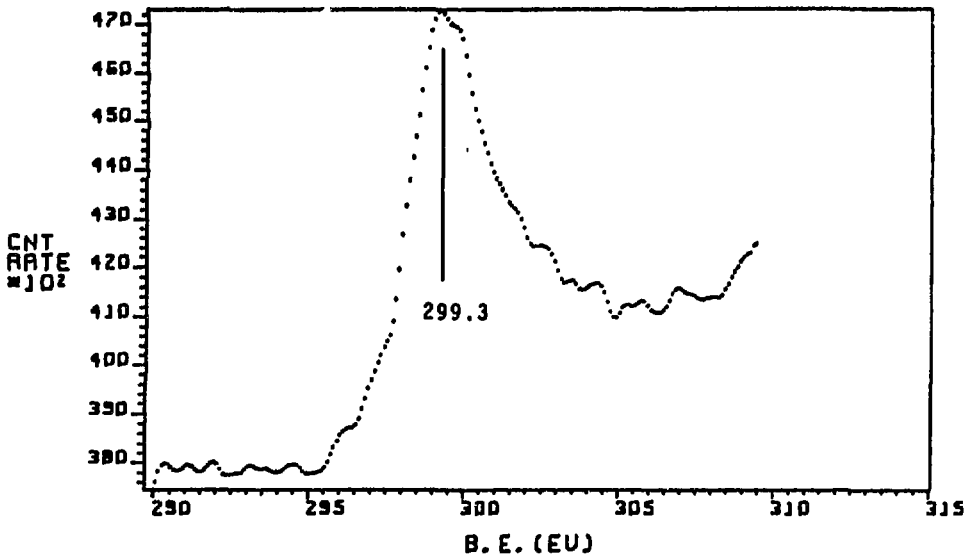

Fig. 4 Y3p XPS spectrum of Y_{fl}.

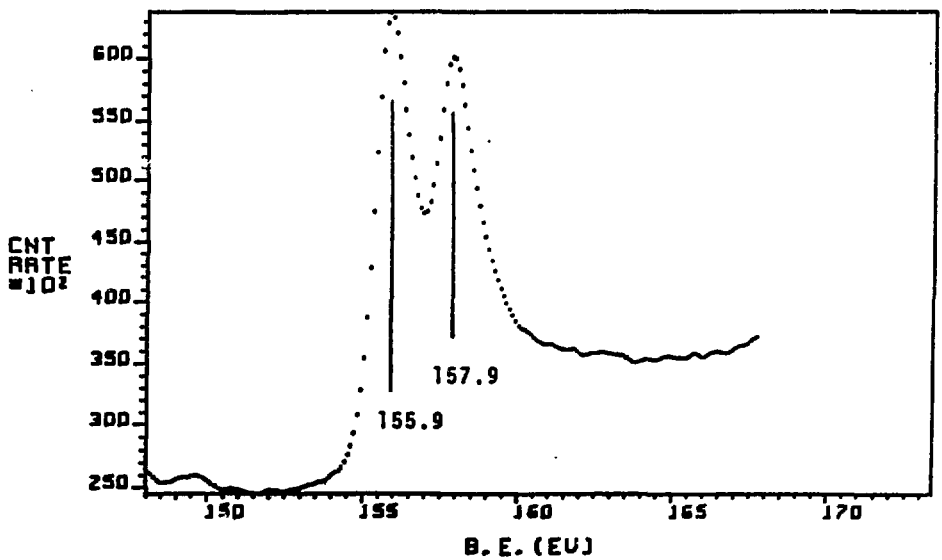

Fig. 5 Y3d XPS spectrum of Y_{fl}.

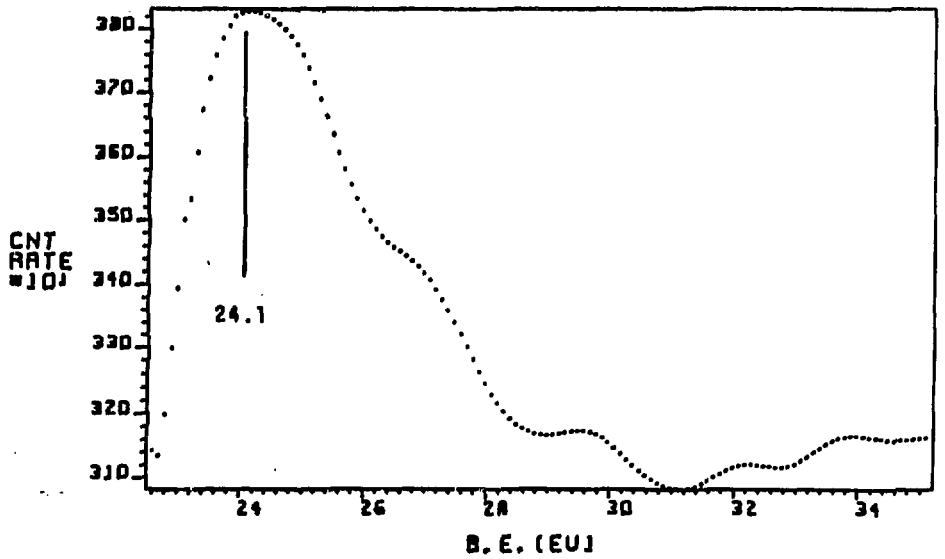

Fig. 6 Y4p XPS spectrum of Y_{fl}.

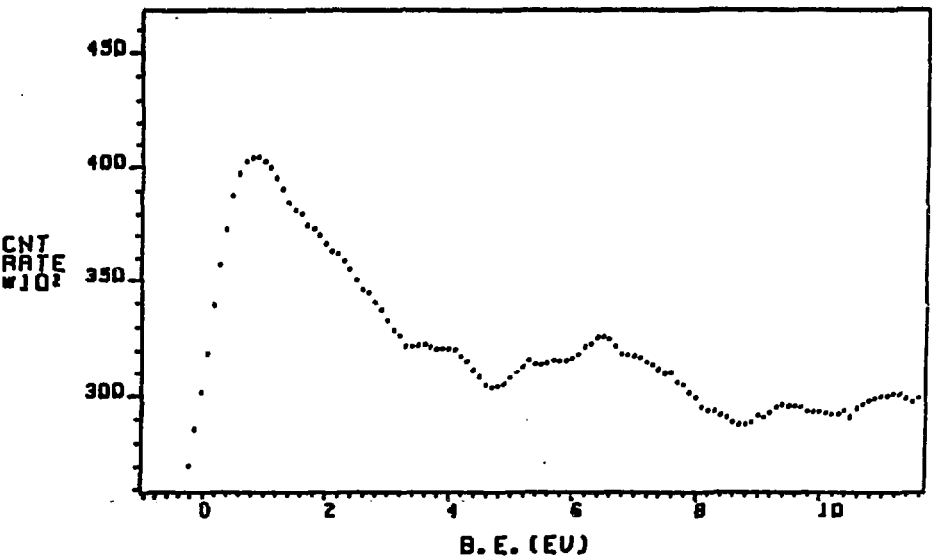

Fig. 7 Valence-band spectrum of Y_{fl}.

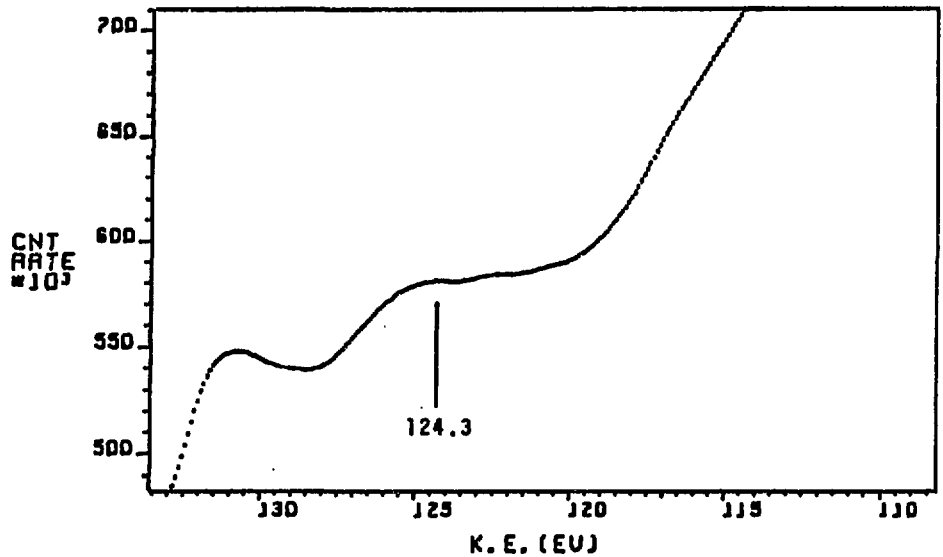

Fig. 8 $M_{4,5}N_{2,3}V$ XAES spectrum of Y_{fl}.

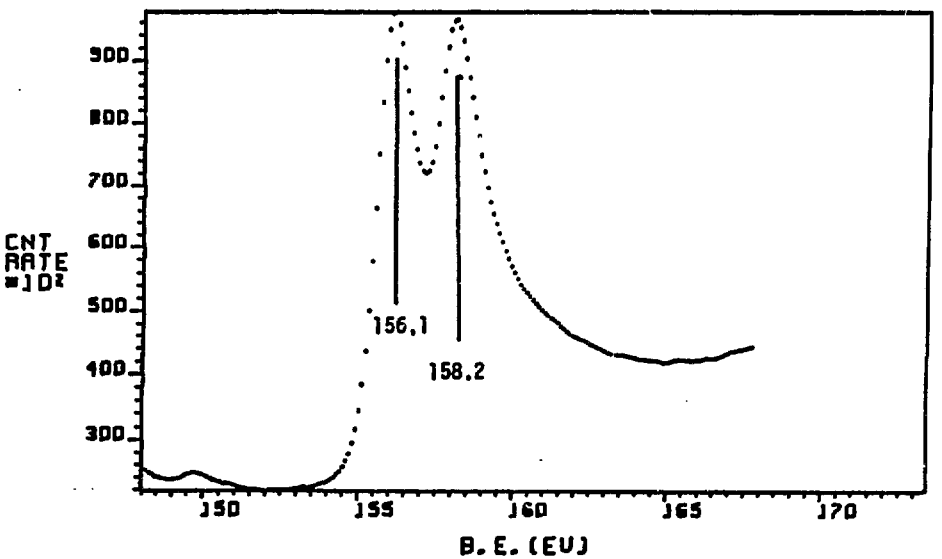

Fig. 9 Y3d XPS spectrum of Y_{et}.

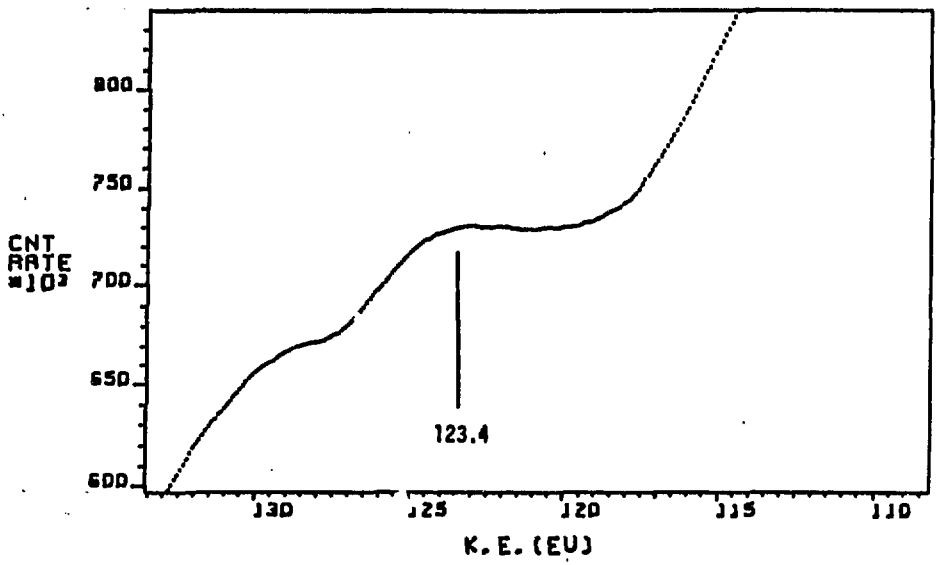

Fig. 10 $M_{4,5}N_{2,3}V$ XAES spectrum of Y_{et}.

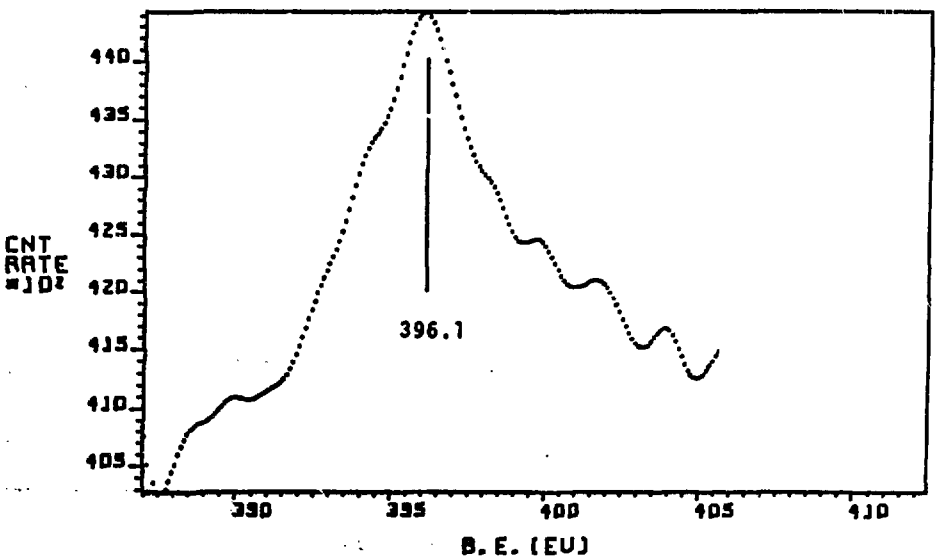

Fig. 11 Y3s XPS spectrum of Y_2O_3.

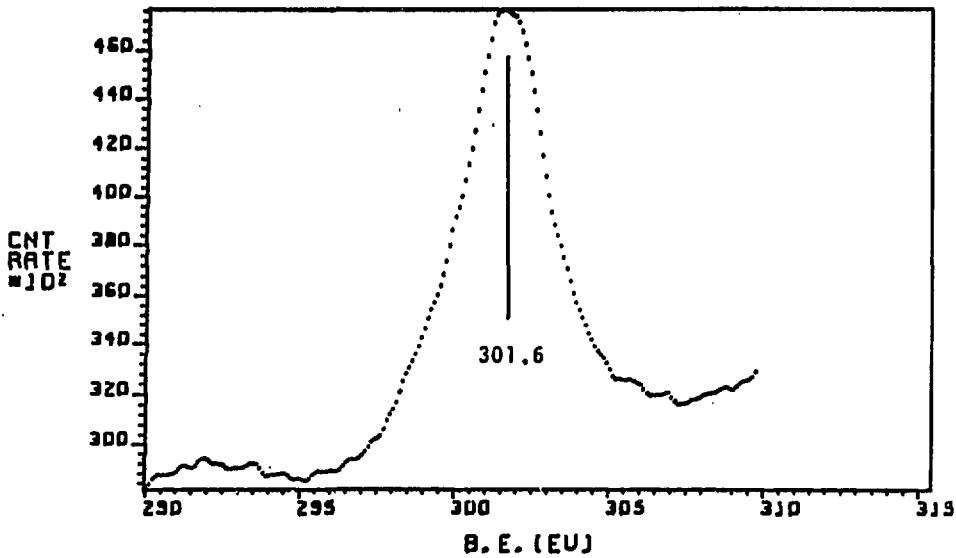

Fig. 12 Y3p XPS spectrum of Y_2O_3.

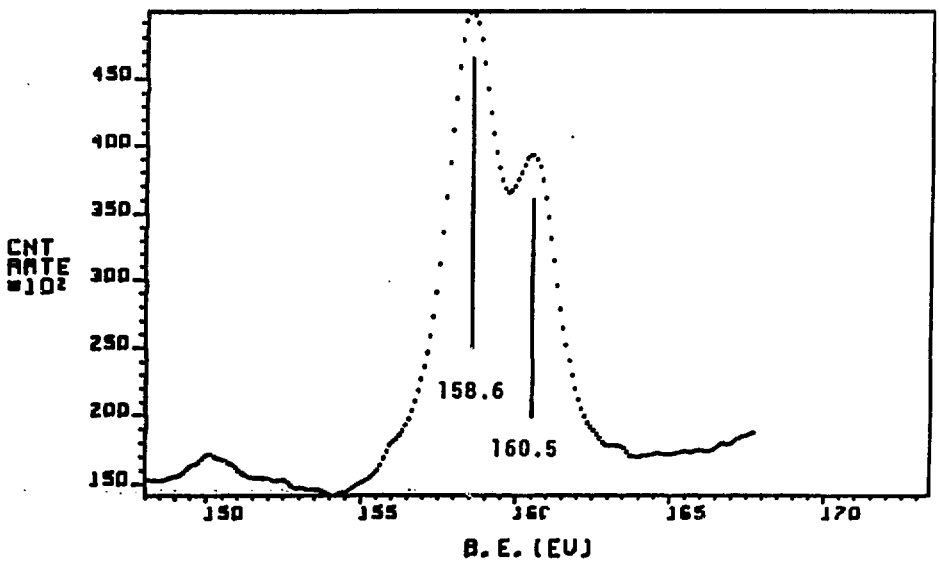

Fig. 13 Y3d XPS spectrum of Y_2O_3.

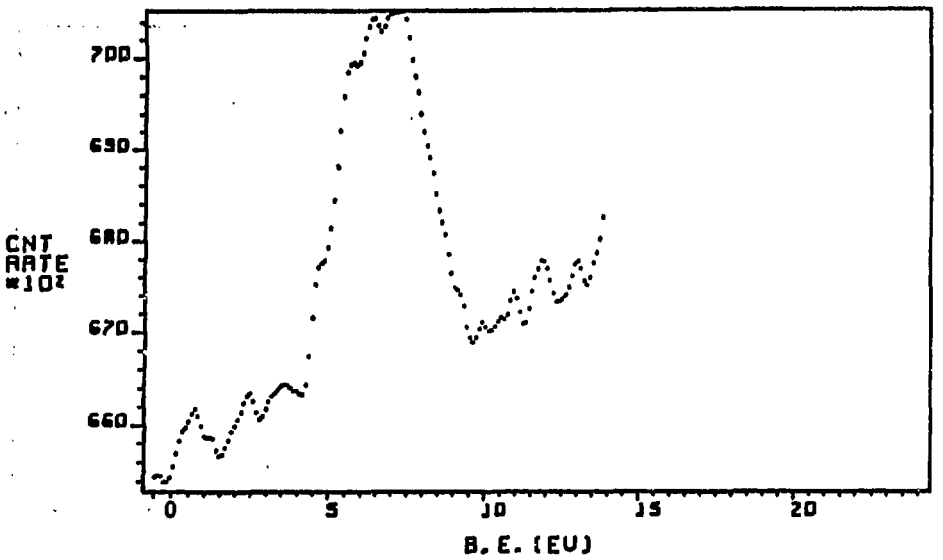

Fig. 14 Valence-band spectrum of Y_2O_3.

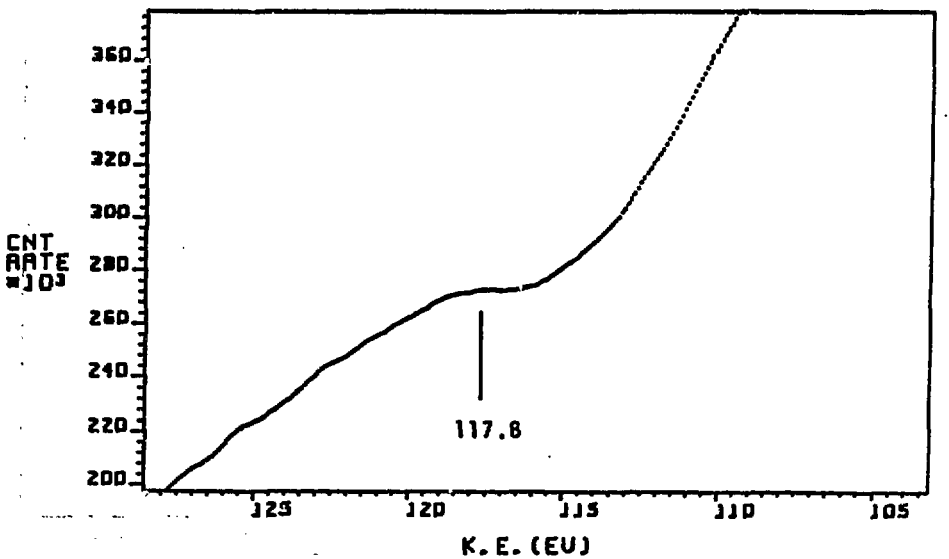

Fig. 15 $M_{4,5}N_{2,3}V$ XAES spectrum of Y_2O_3.

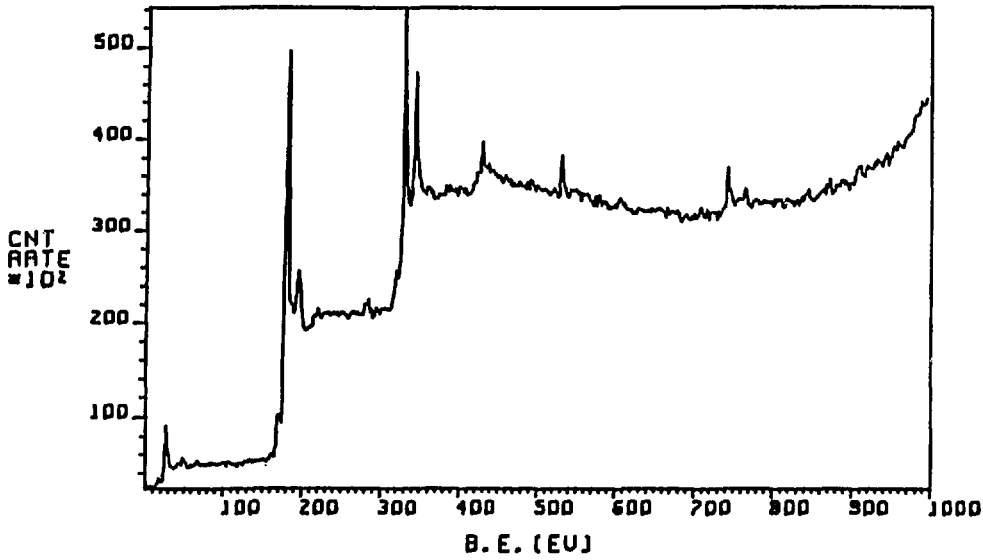

Fig. 16 XPS wide scan of Zr_{fl}.

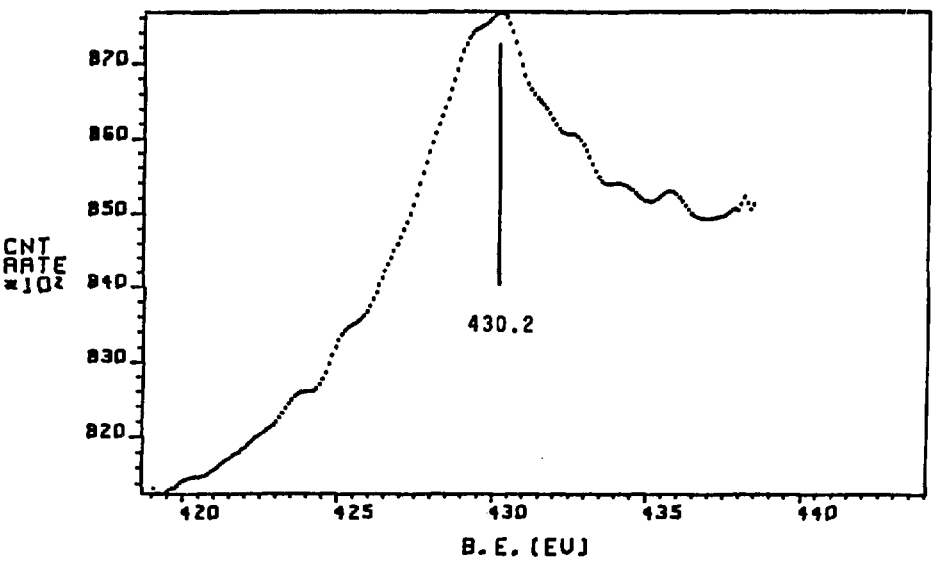

Fig. 17 Zr3s XPS spectrum of Zr_{fl}.

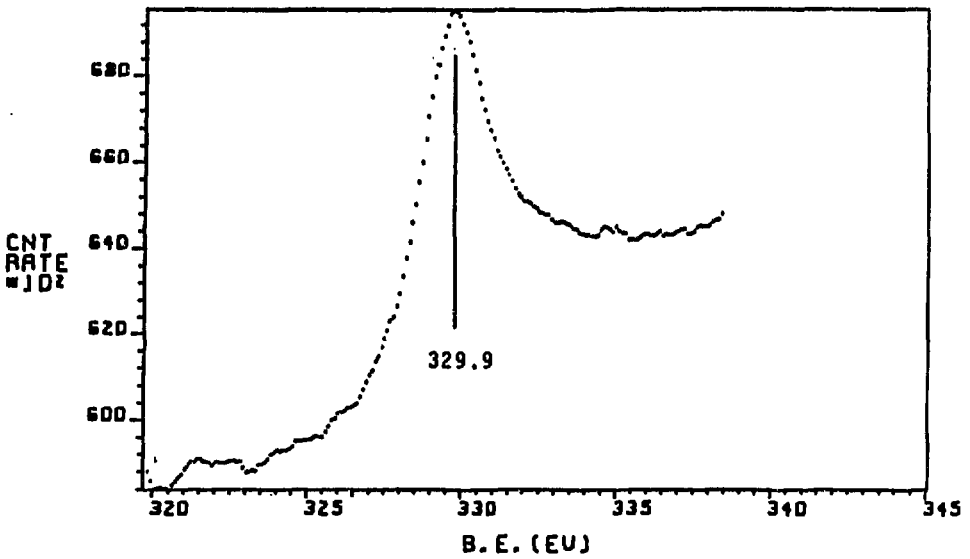

Fig. 18 Zr3p XPS spectrum of Zr_{fl}.

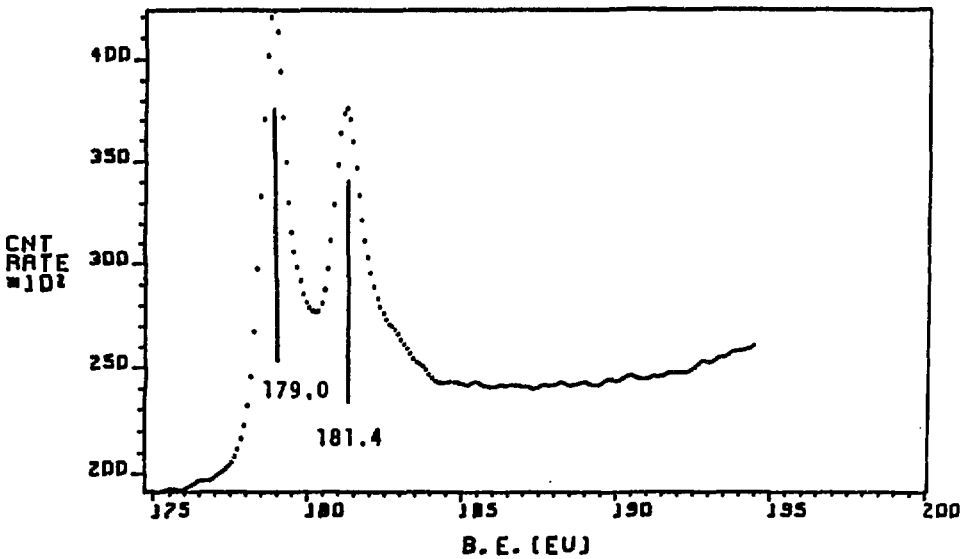

Fig. 19 Zr3d XPS spectrum of Zr_{fl}.

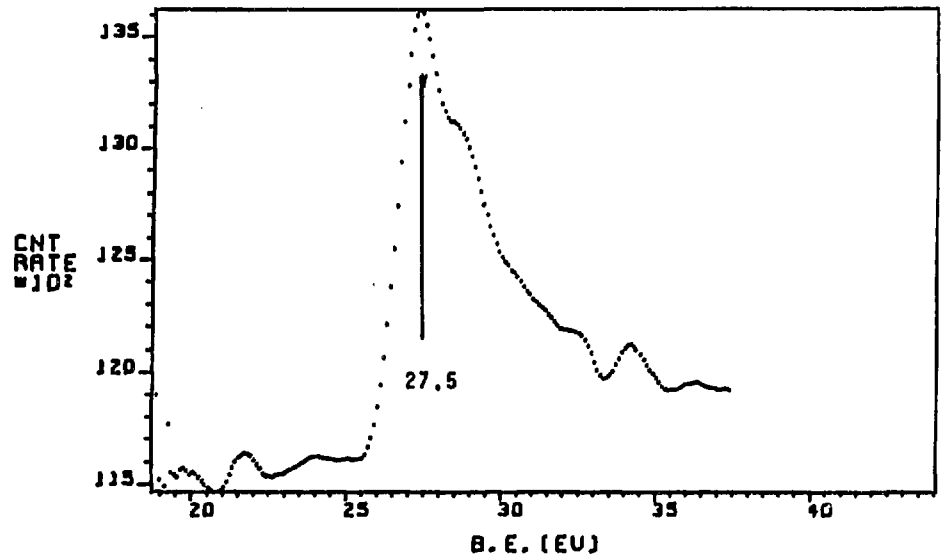

Fig. 20 Zr4p XPS spectrum of Zr_{fl}.

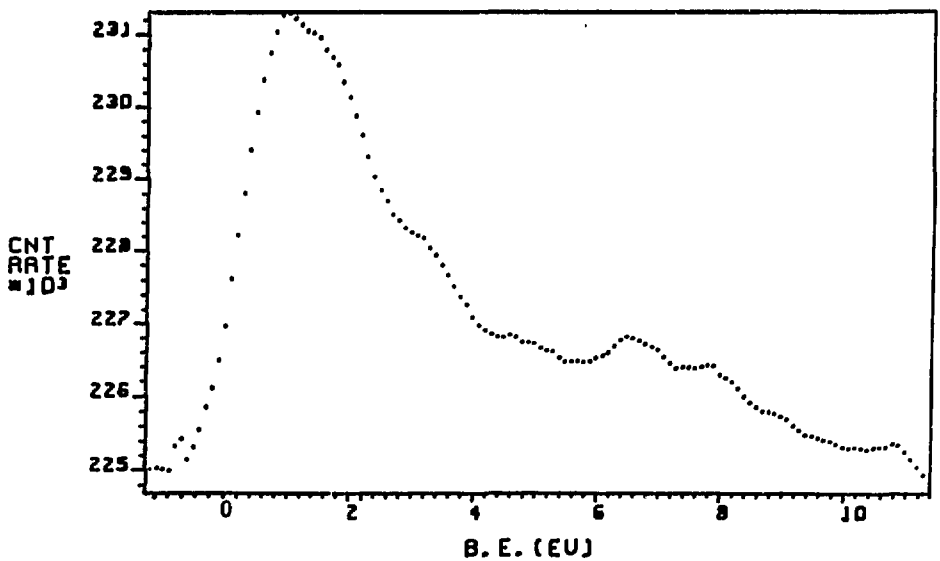

Fig. 21 Valence-band spectrum of Zr_{fl}.

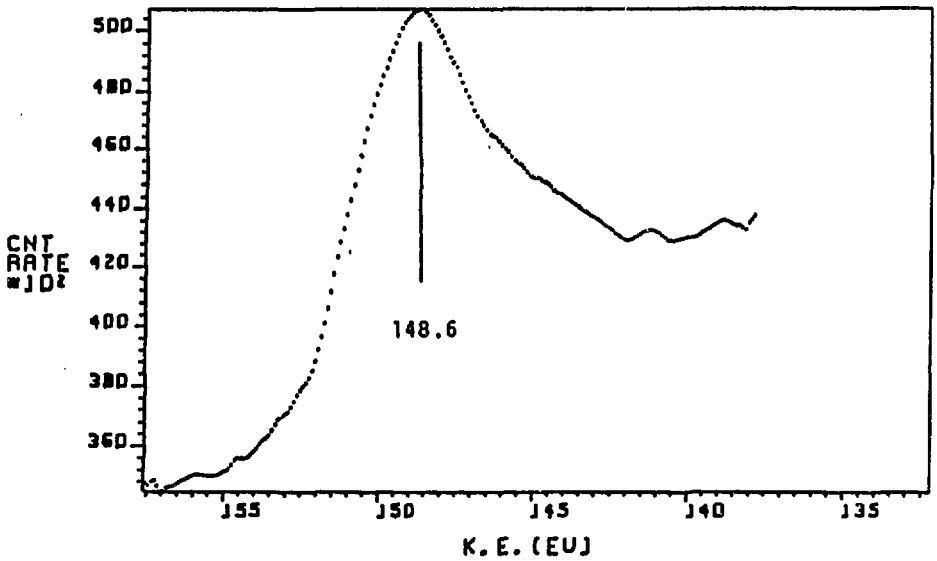

Fig. 22 $M_{4,5}N_{2,3}V$ XAES spectrum of Zr_{fl}.

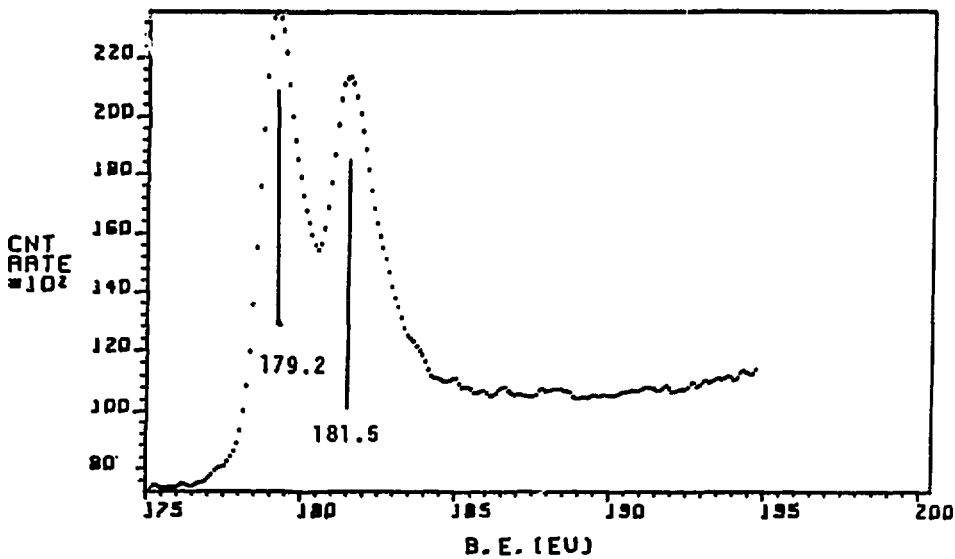

Fig. 23 Zr3d XPS spectrum of Zr_{et}.

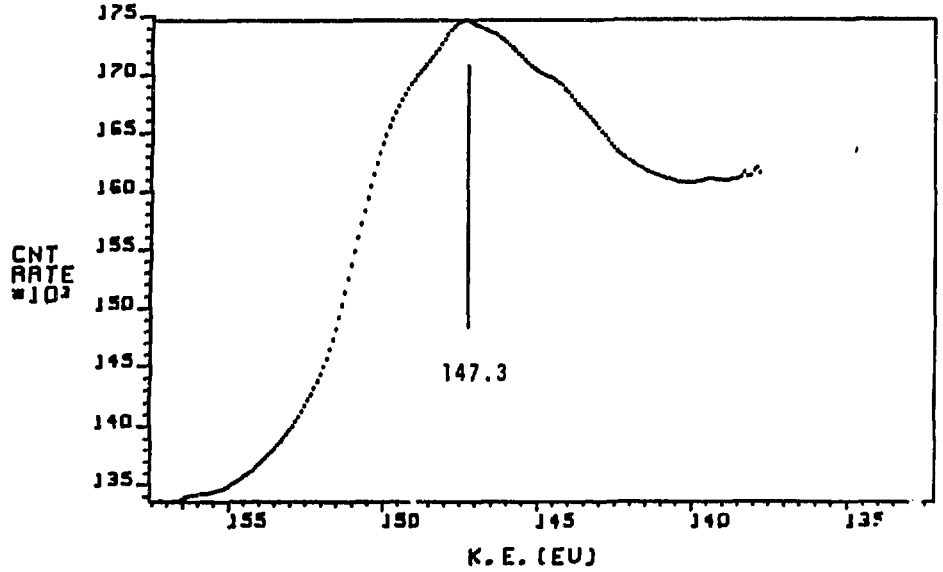

Fig. 24 $M_{4,5}N_{2,3}V$ XAES spectrum of Zr_{et}.

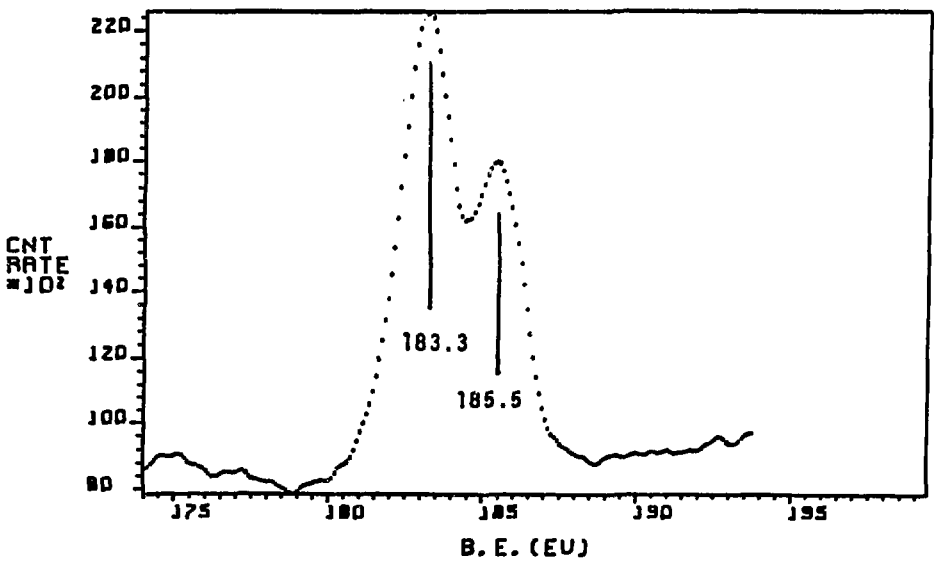

Fig. 25 Zr3d XPS spectrum of ZrO_2.

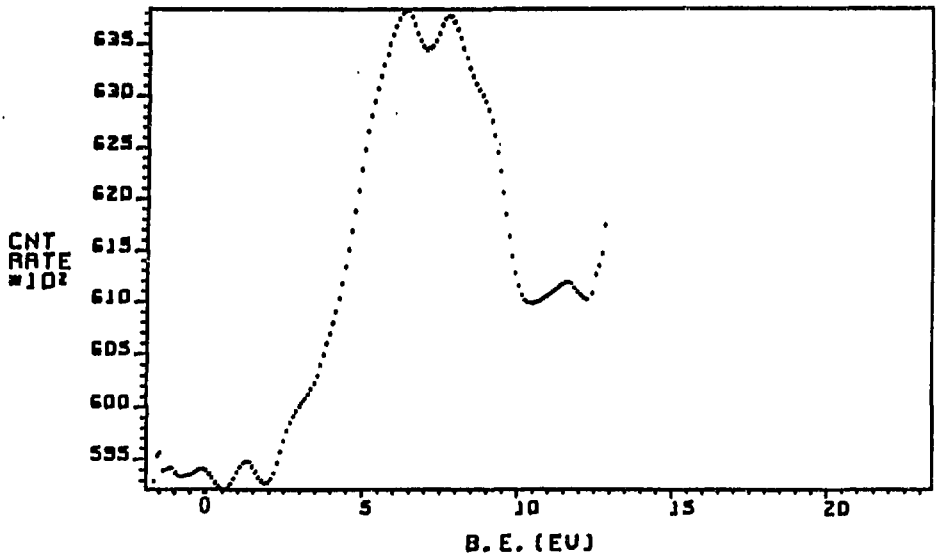

Fig. 26 Valence-band spectrum of ZrO_2.

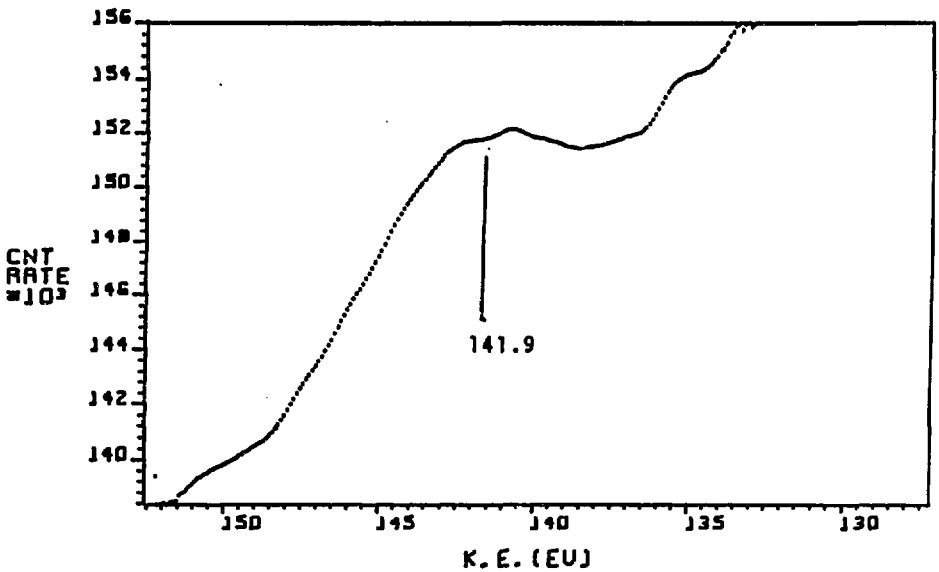

Fig. 27 $M_{4,5}N_{2,3}V$ XAES spectrum of ZrO_2.

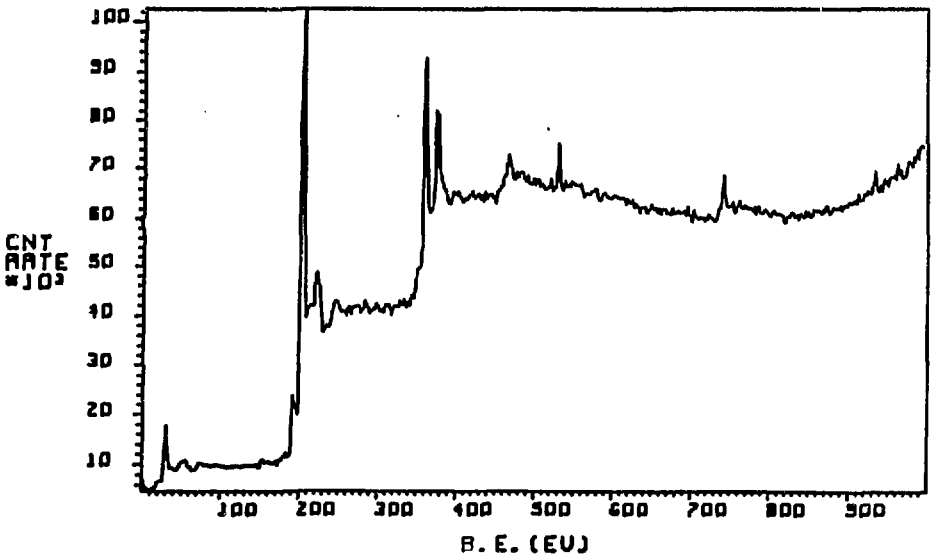

Fig. 28 XPS wide scan of Nb_{fl}.

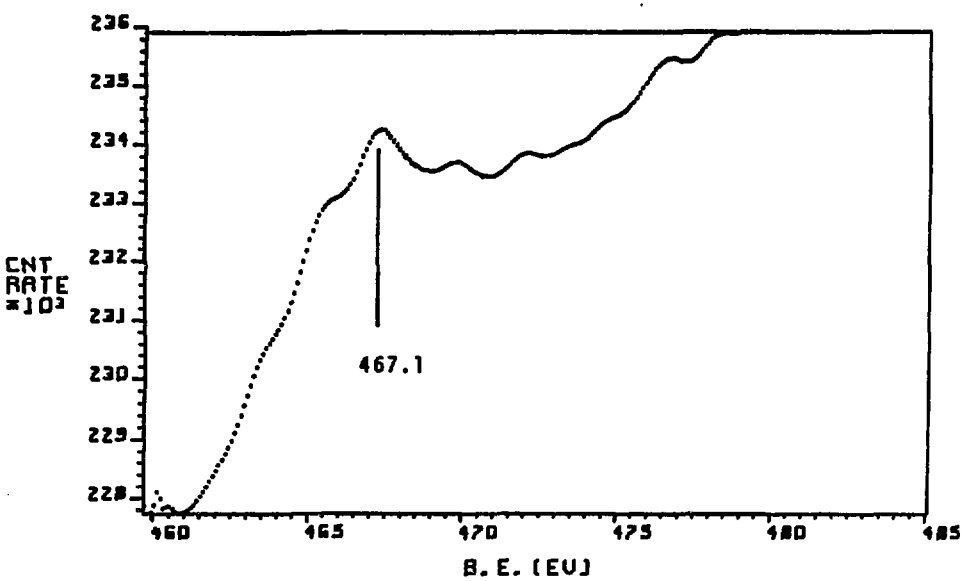

Fig. 29 Nb3s XPS spectrum of Nb_{fl}.

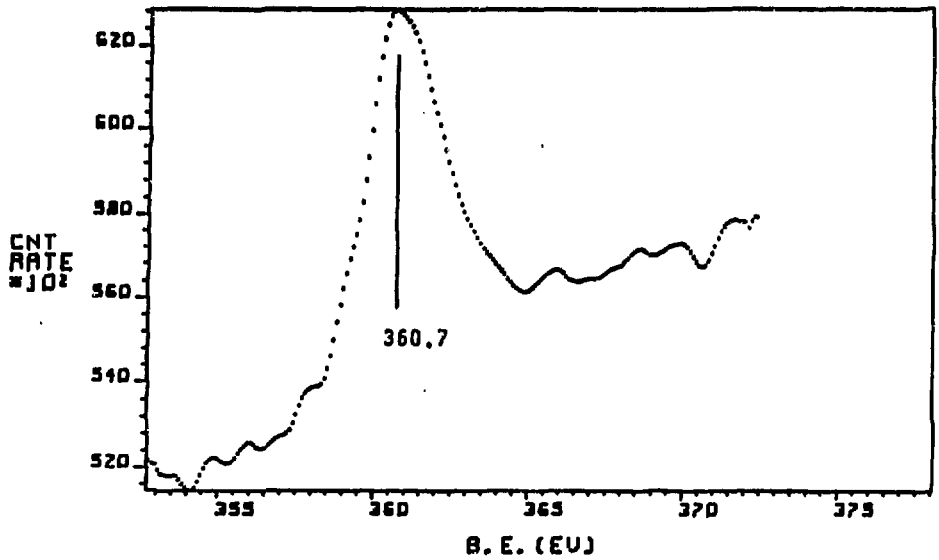

Fig. 30 Nb3p XPS spectrum of Nb_{fl}.

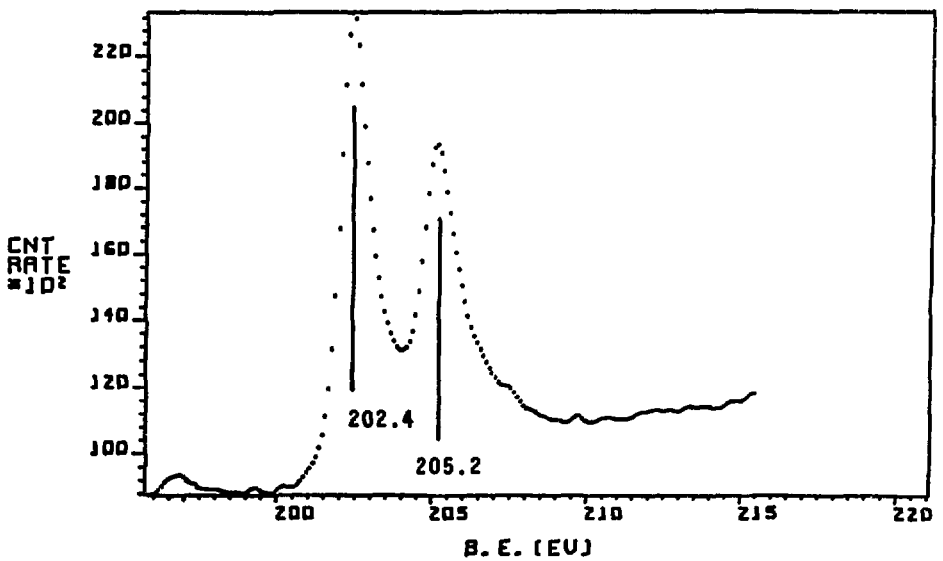

Fig. 31 Nb3d XPS spectrum of Nb_{fl}.

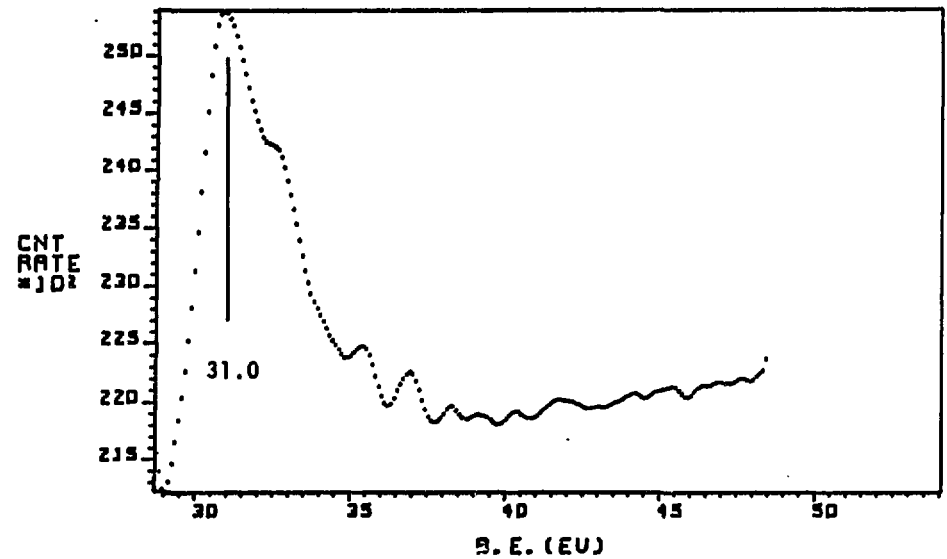

Fig. 32 Nb4p XPS spectrum of Nb_{fl}.

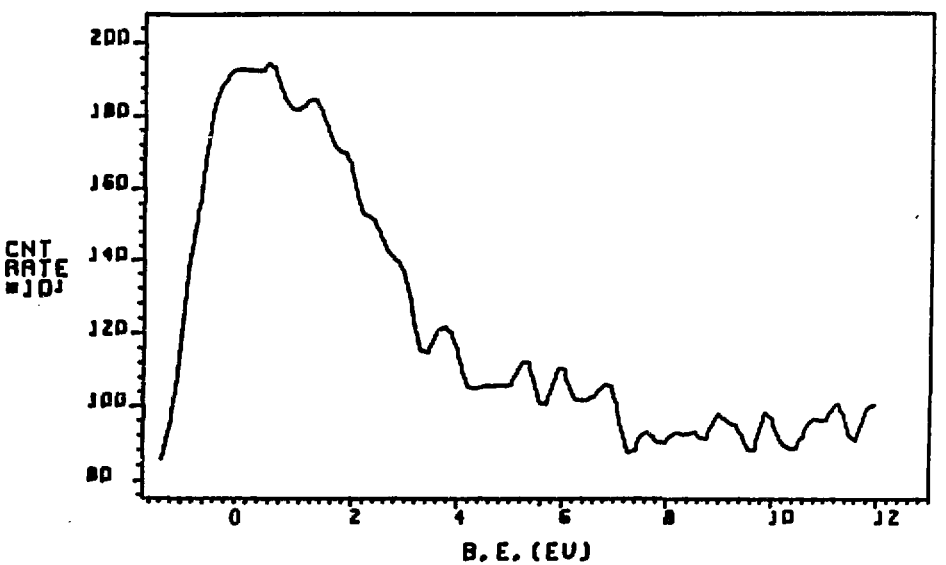

Fig. 33 Valence-band spectrum of Nb_{fl}.

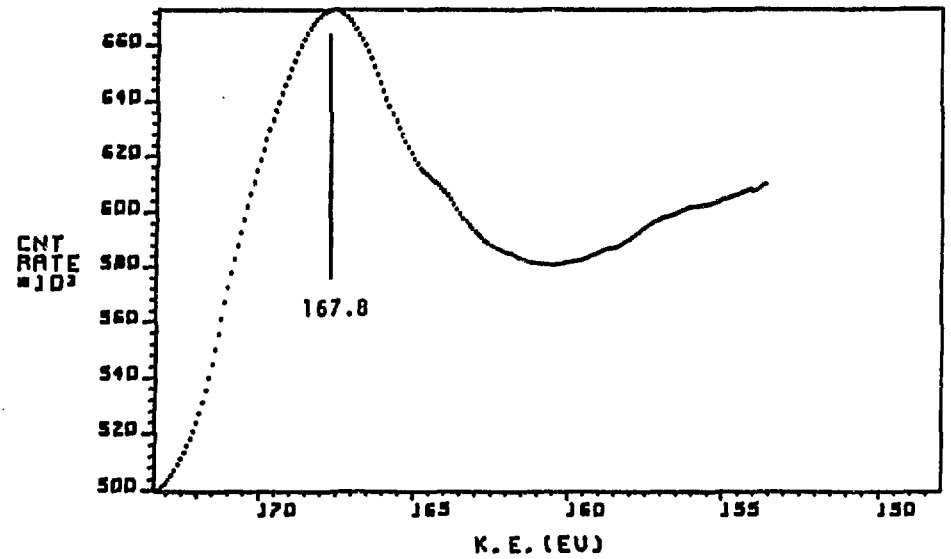

Fig. 34 $M_{4,5}N_{2,3}V$ XAES spectrum of Nb_{fl}.

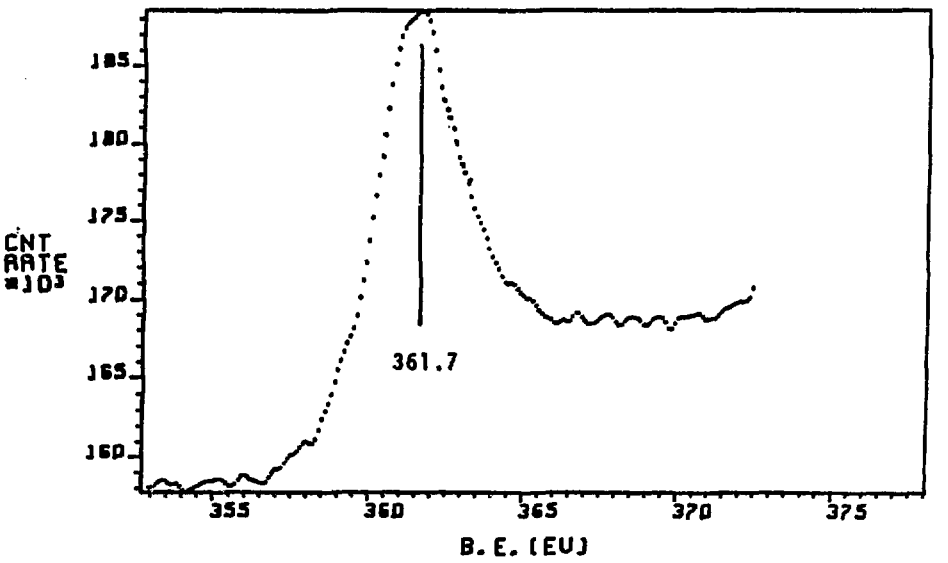

Fig. 35 Nb3p XPS spectrum of Nb_{et}.

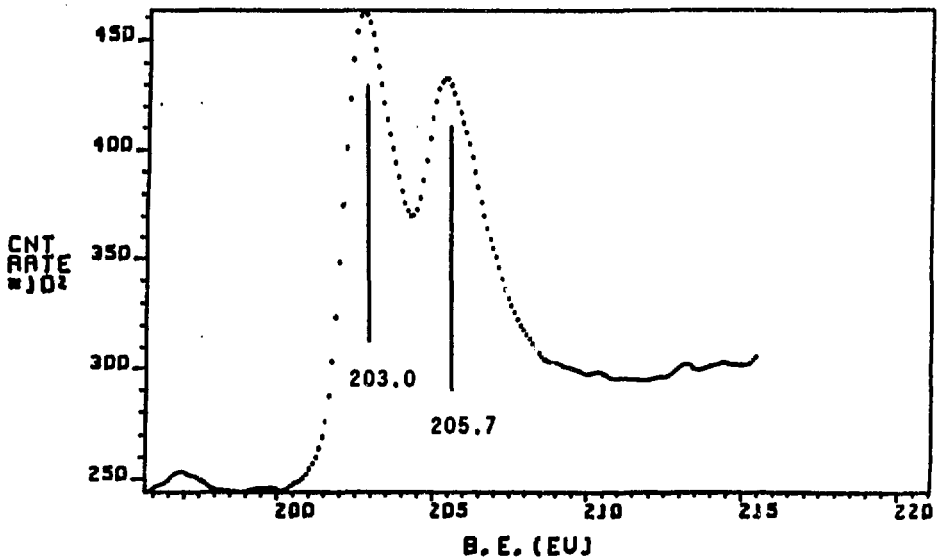

Fig. 36 Nb3d XPS spectrum of Nb_{et}.

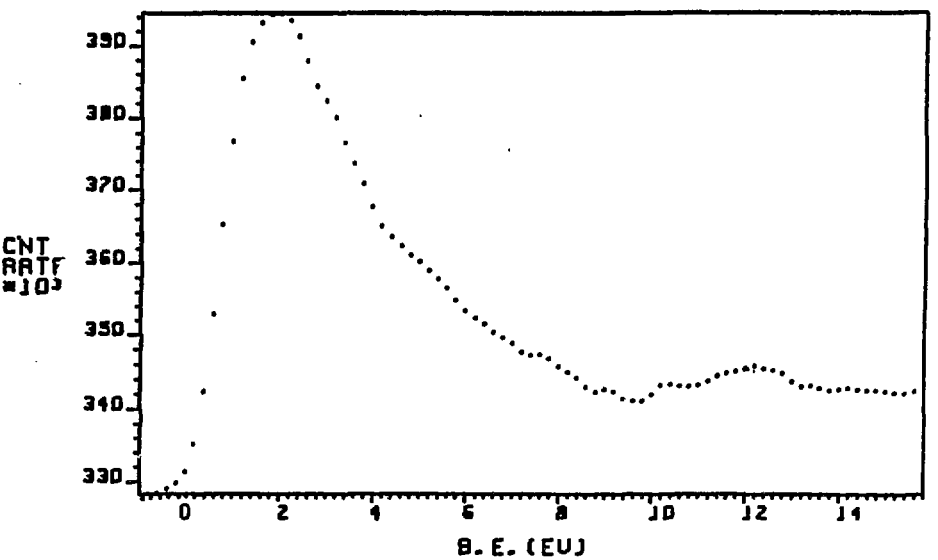

Fig. 37 Valence-band spectrum of Nb_{et}.

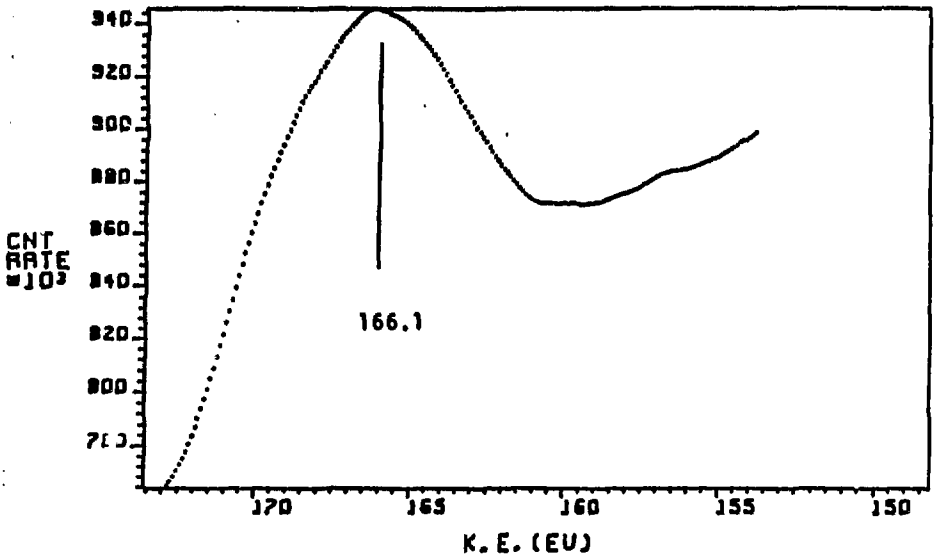

Fig. 38 $M_{4,5}N_{2,3}V$ XAES spectrum of Nb_{et}.

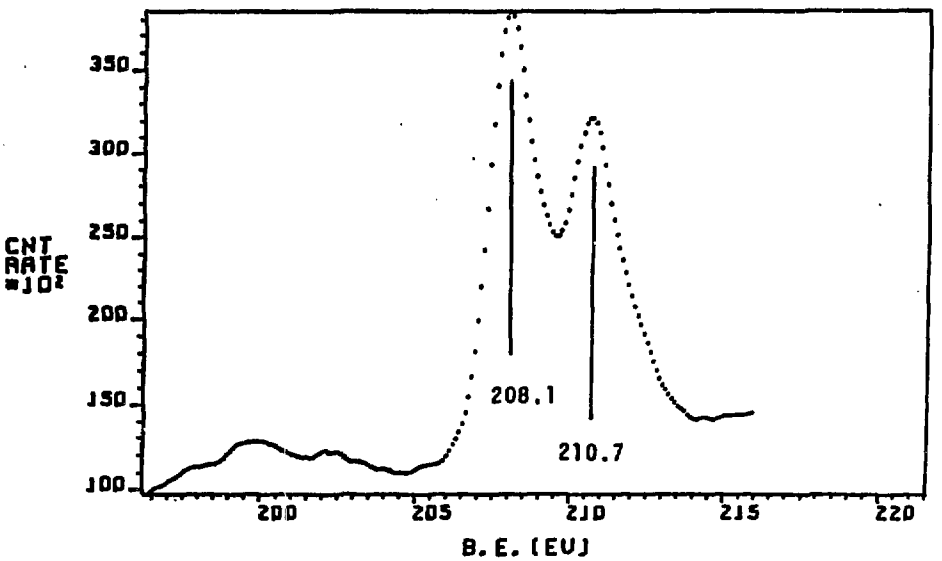

Fig. 39 Nb3d XPS spectrum of Nb_2O_5.

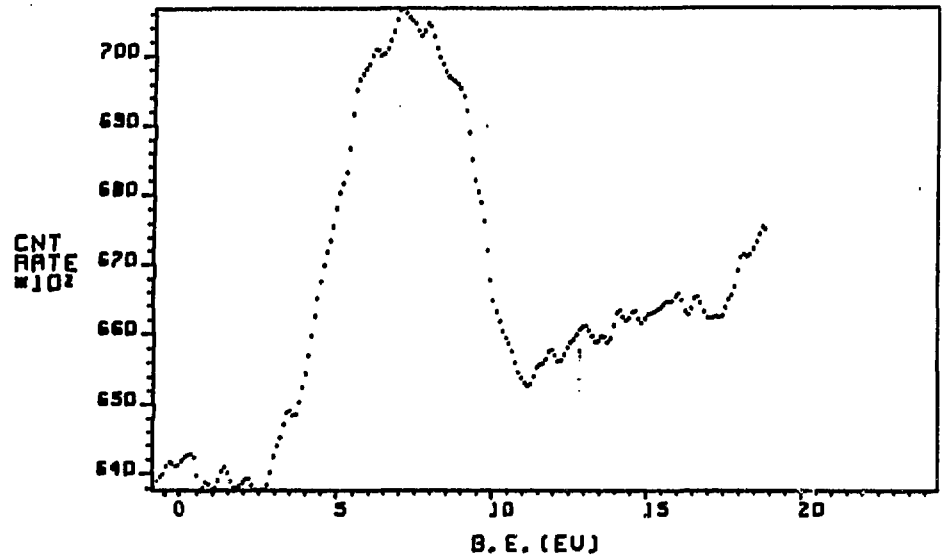

Fig. 40 Valence-band spectrum of Nb_2O_5.

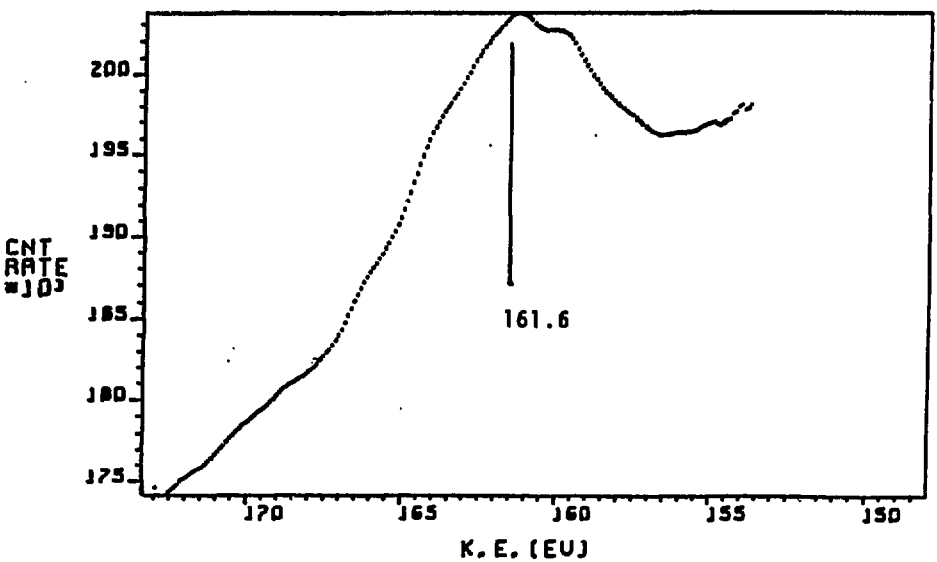

Fig. 41 $M_{4,5}N_{2,3}V$ XAES spectrum of Nb_2O_5.

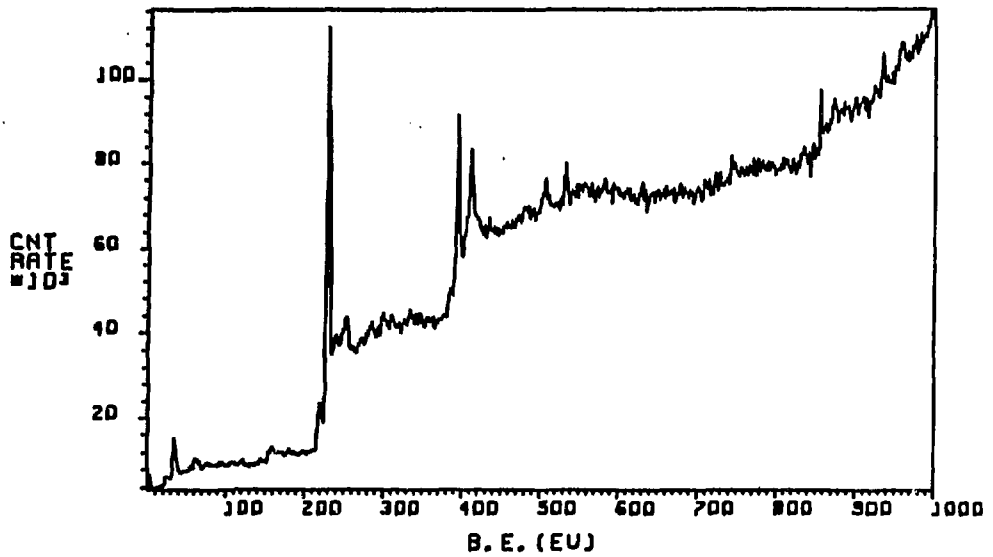

Fig. 42 XPS wide scan of Mo_{fl}.

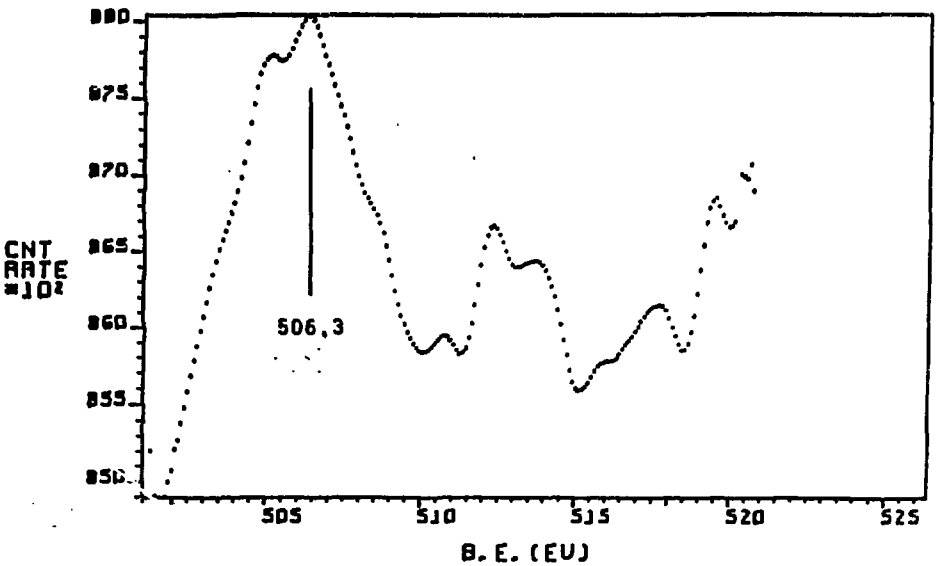

Fig. 43 Mo3s XPS spectrum of Mo_{fl}.

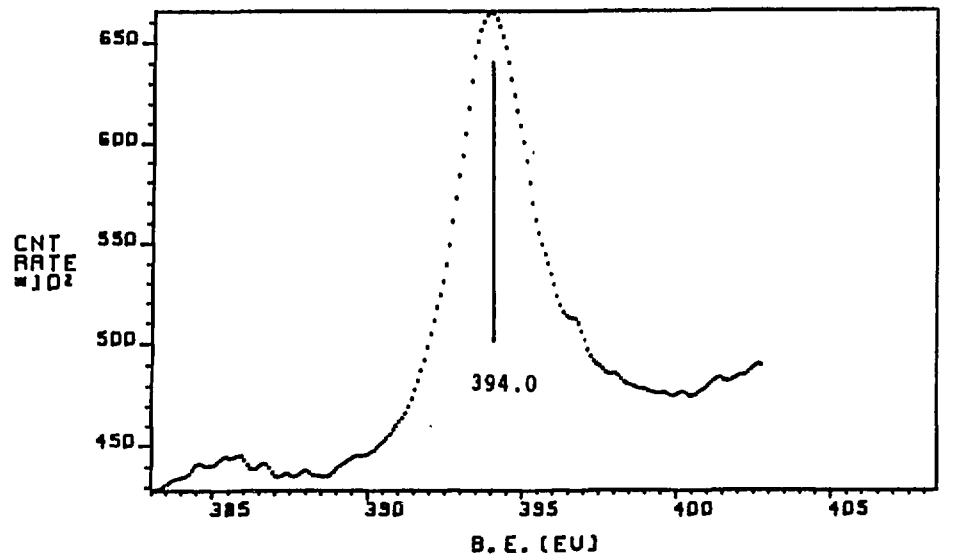

Fig. 44 Mo3p XPS spectrum of Mo_{fl}.

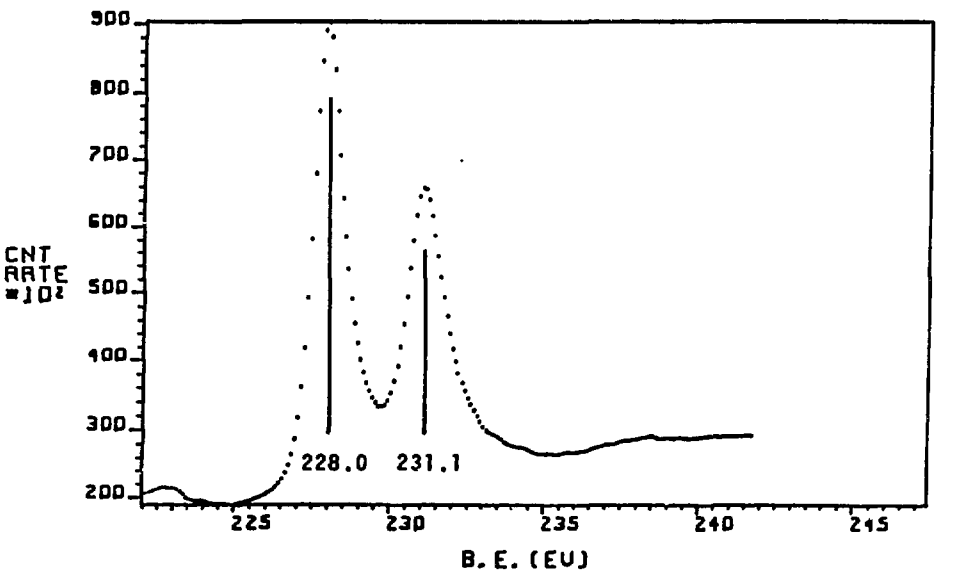

Fig. 45 Mo3d XPS spectrum of Mo_{fl}.

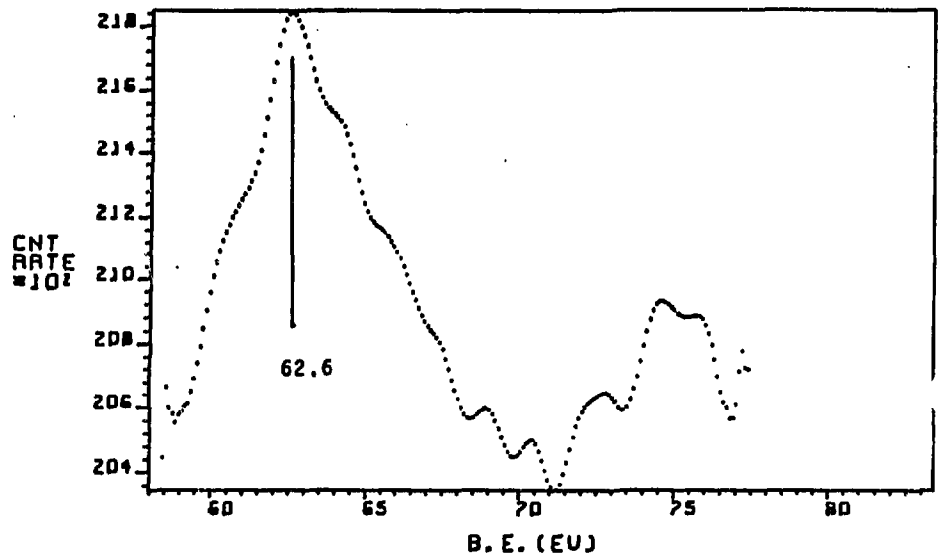

Fig. 46 Mo4s XPS spectrum of Mo_{fl}.

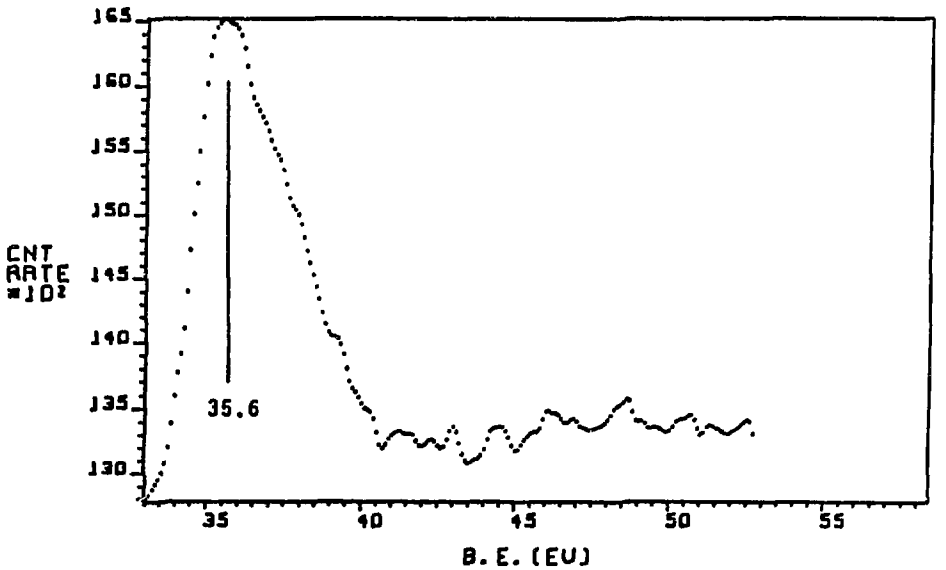

Fig. 47 Mo4p XPS spectrum of Mo_{fl}.

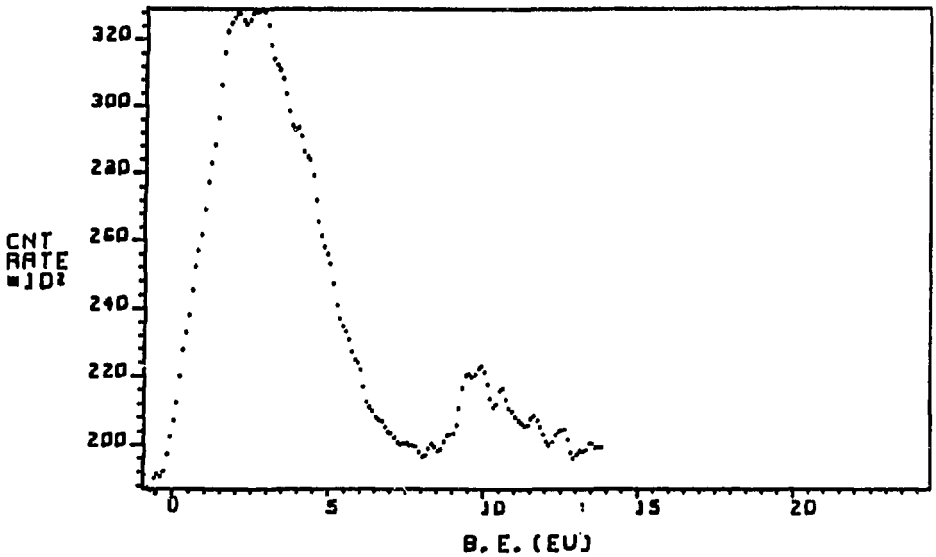

Fig. 48 Valence-band spectrum of Mo_{fl}.

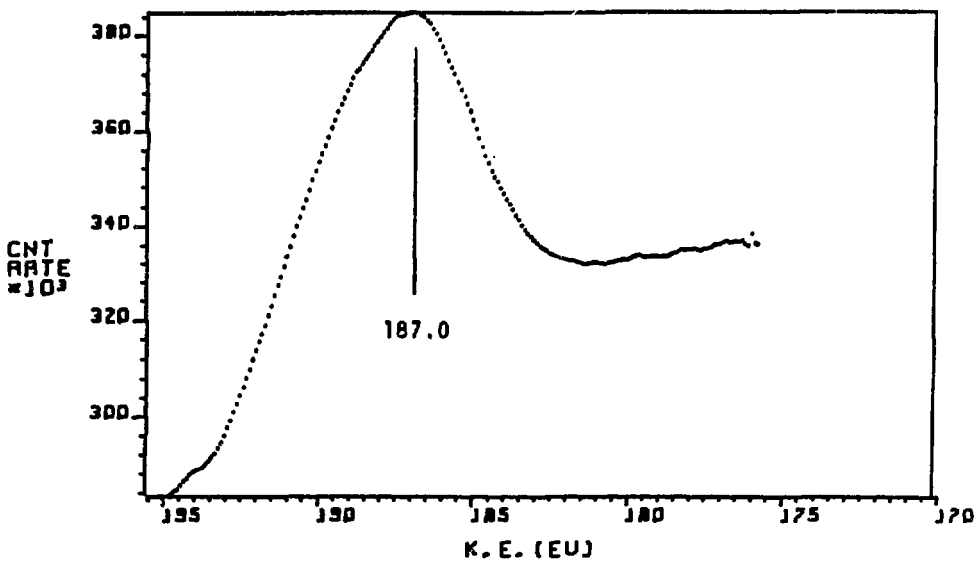

Fig. 49 $M_{4,5}N_{2,3}V$ XAES spectrum of Mo_{fl}.

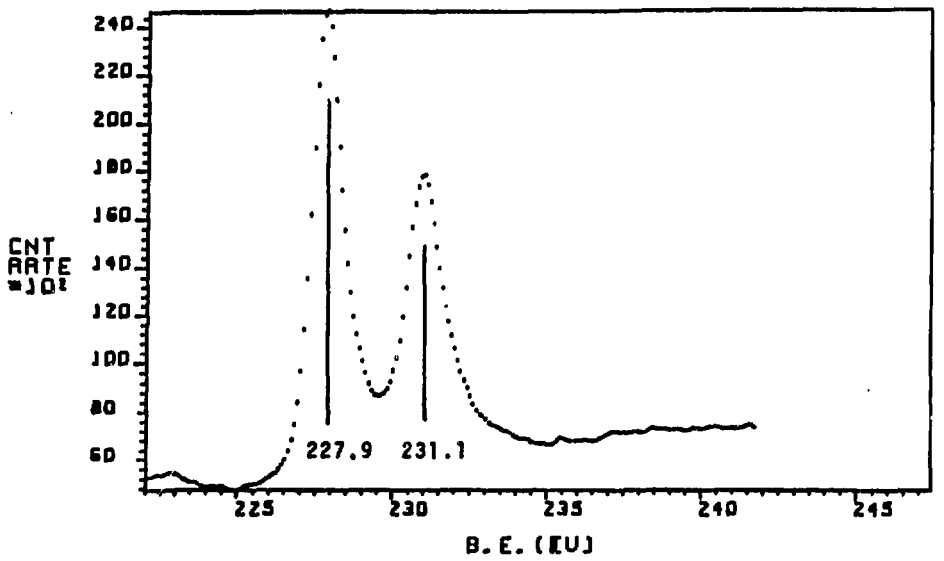

Fig. 50 Mo3d XPS spectrum of Mo_{et}.

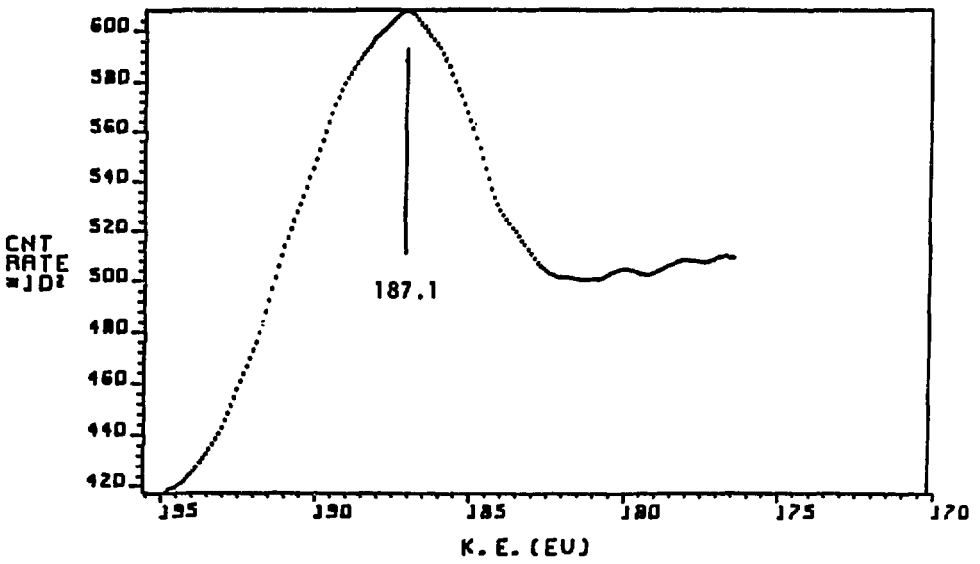

Fig. 51 $M_{4,5}N_{2,3}V$ XAES spectrum of Mo_{et}.

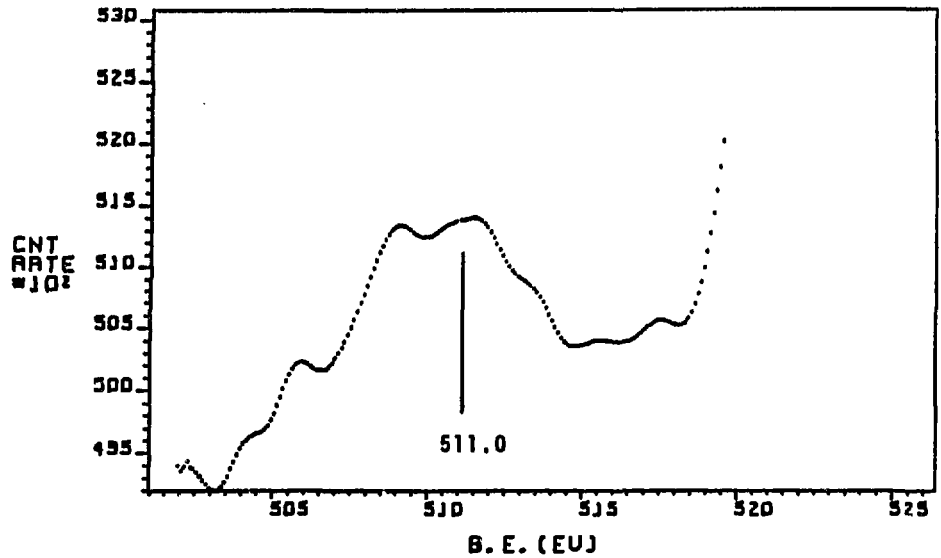

Fig. 52 Mo3s XPS spectrum of MoO_3.

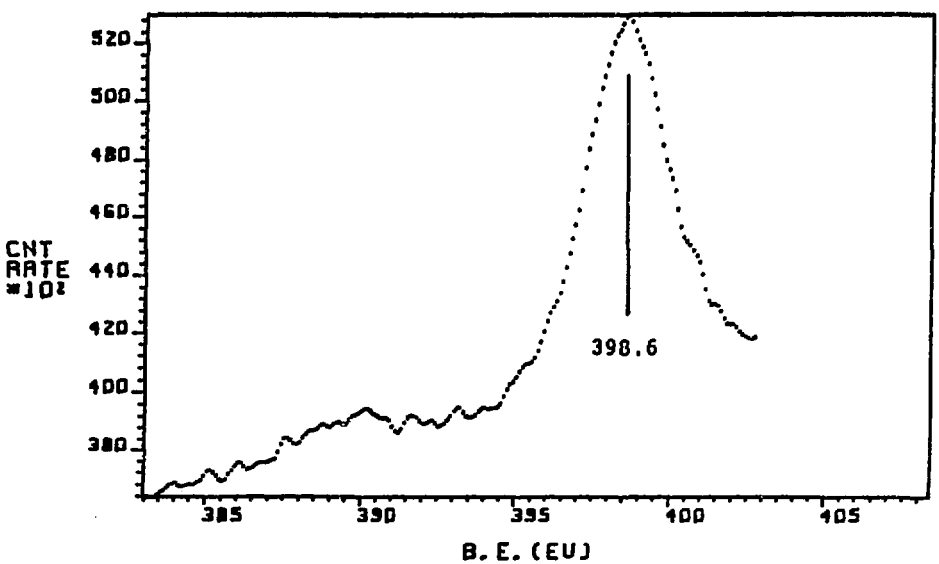

Fig. 53 Mo3p XPS spectrum of MoO_3.

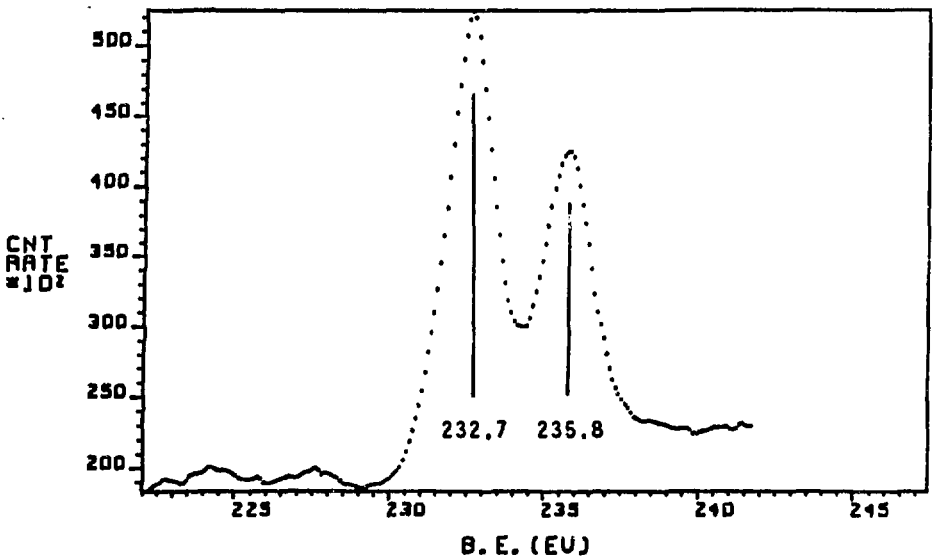

Fig. 54 Mo3d XPS spectrum of MoO_3.

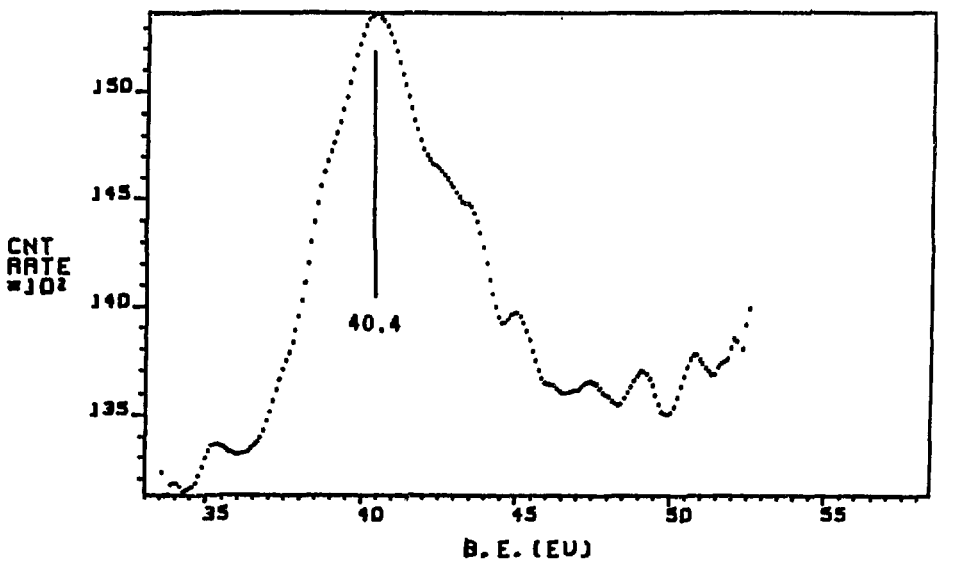

Fig. 55 Mo4p XPS spectrum of MoO_3.

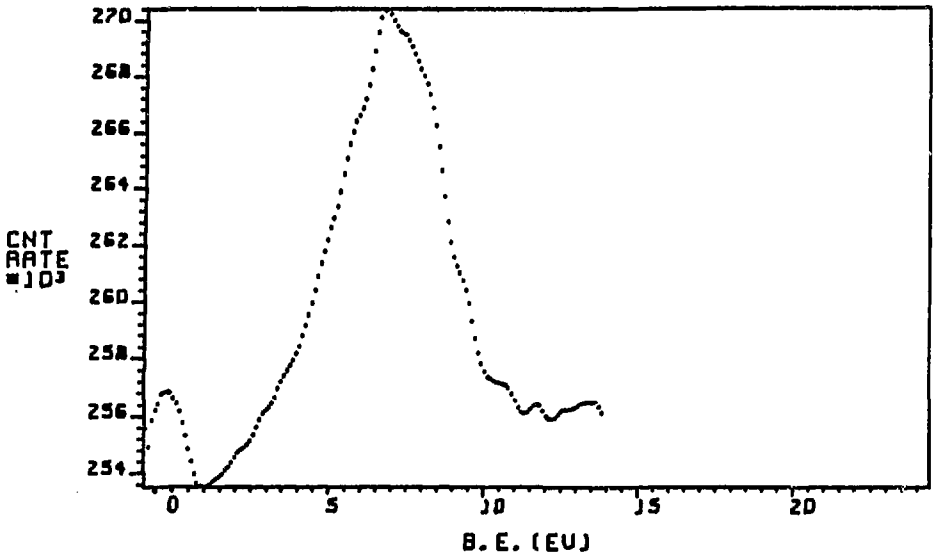

Fig. 56 Valence-band spectrum of MoO_3.

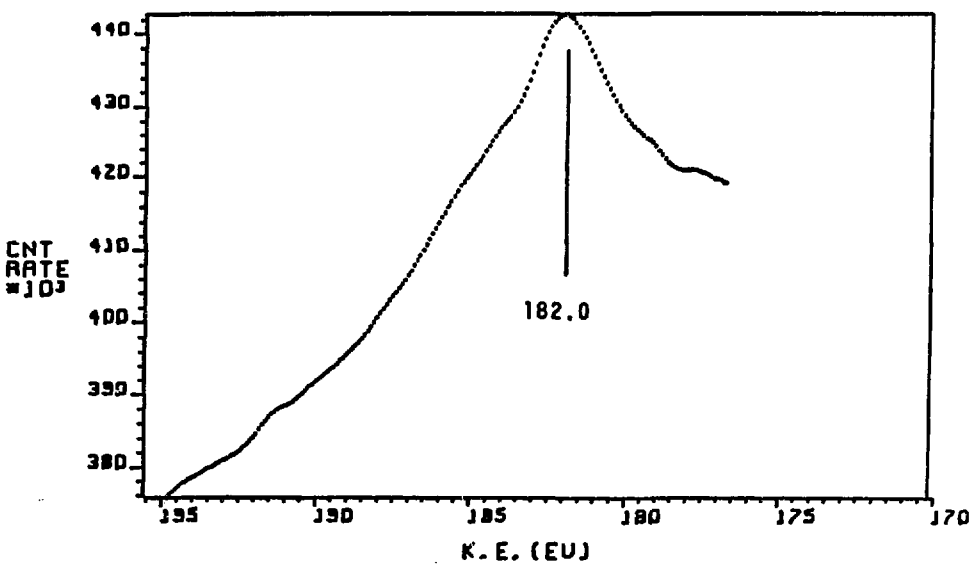

Fig. 57 $M_{4,5}N_{2,3}V$ XAES spectrum of MoO_3.

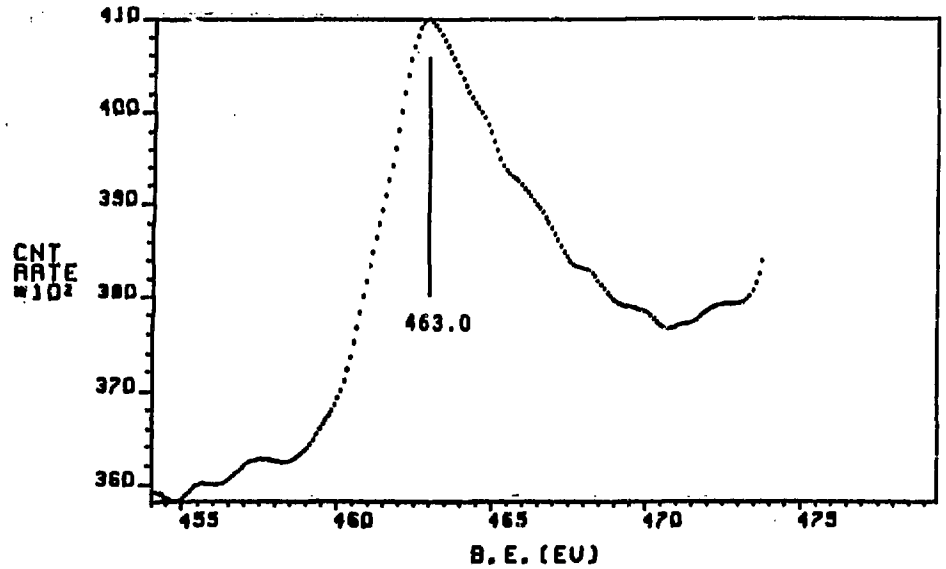

Fig. 58 Ru3p XPS spectrum of RuO_2.

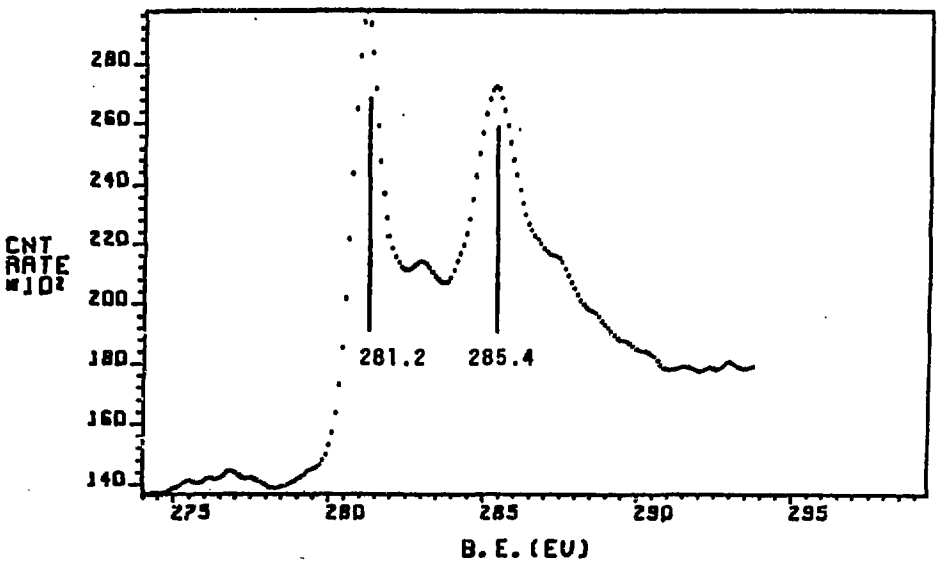

Fig. 59 Ru3d XPS spectrum of RuO_2.

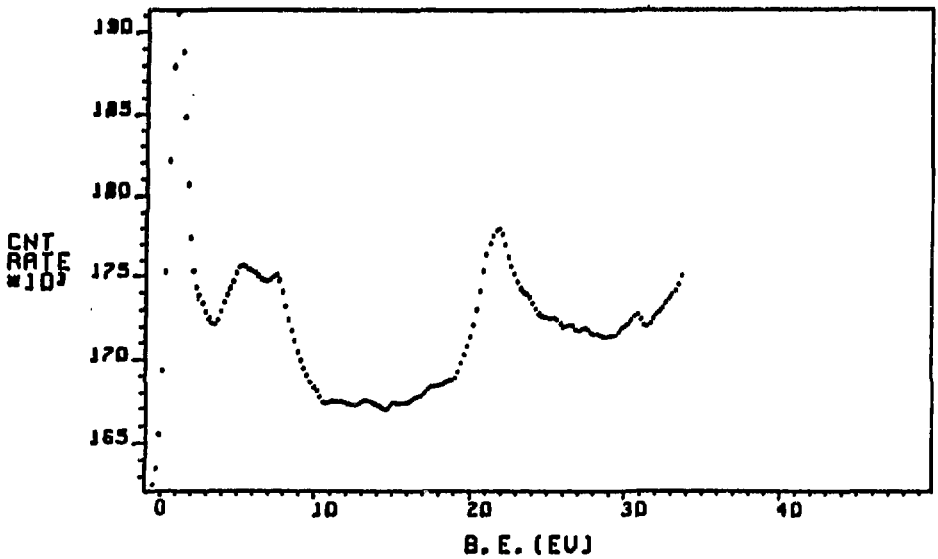

Fig. 60 Valence-band spectrum of RuO_2.